

# Assessment of the water mass dynamics over the western Mediterranean in the MEDRYS1V2 reanalysis

Quentin-Boris Barral<sup>1</sup>, Bruno Agop Zakardjian<sup>2</sup>, Franck DUMAS<sup>3</sup>, Pierre GARREAU<sup>4</sup>, and Jonathan Beuvier<sup>5</sup>

<sup>1</sup>Université de Toulon

<sup>2</sup>Mediterranean Institute of Oceanography

<sup>3</sup>SHOM

<sup>4</sup>Ifremer

<sup>5</sup>CNRM, Météo-France/CNRS

August 4, 2023

## Abstract

We present an assessment of the water mass dynamics in a reanalysis of the Mediterranean Sea with a focus on the Western basin. We use a  $\vartheta$ -S based algorithm to compute the fractions of the main western Mediterranean water masses : Atlantic and modified Atlantic Waters (AW, mAW), Western and Levantine Intermediate Waters (WIW and LIW) and Western Mediterranean Deep Waters (WDW). The reanalysis retains the known mean characteristics of the water masses, their seasonal to interannual variability and main circulation patterns when compared with the literature. The imprints of winter mixing is particularly obvious with coherent variations of water mass volumes, mainly the yearly creation of WIW from mAW on northernmost shelves and of WMDW from all surface and intermediate layers during years of deep water formation. The results also highlight some unrealistic events of variability of the WMDW volume that are likely due to the data assimilation process. Re-computing the water mass volumes and transports without these altered years allowed to highlight the possible disruption of the large-scale barotropic cyclonic circulation in the Eastern Algerian basin in response to major DWF events over the Gulf of Lion. The reanalysis also shows an overtopping of WMDW in the Sardinia Channel in 2009 leading to a major backward flow of mAW from the Tyrrhenian to the Algero-Provençal basin. Both processes affect the circulations of AW and mAW over the whole western Mediterranean.

## Hosted file

969037\_0\_art\_file\_11231019\_ryg8n8.docx available at <https://aurelia.com/users/287119/articles/658115-assessment-of-the-water-mass-dynamics-over-the-western-mediterranean-in-the-medrys1v2-reanalysis>

1 **Assessment of the water mass dynamics over the western Mediterranean in**  
2 **the MEDRYS1V2 reanalysis**

3

4 Quentin-Boris Barral<sup>1</sup>, Bruno Zakardjian<sup>1</sup>, Franck Dumas<sup>2,3</sup>, Pierre Garreau<sup>3</sup>, Jonathan Beuvier<sup>4</sup>

5

6 <sup>1</sup> Université de Toulon, Aix-Marseille Université, CNRS, IRD, MIO, Toulon, France

7 <sup>2</sup> SHOM, Service Hydrologique et Océanographique de la Marine, 13 rue de Chatelier,

8 CS592803, 29228 Brest CEDEX2, France

9 <sup>3</sup> IFREMER, UNIV. Brest, CNRS UMR 6523, IRD, Laboratoire d'Océanographie Physique et  
10 Spatiale (LOPS), IUEM, 29280, Plouzané, France

11 <sup>4</sup> CNRM, Météo-France/CNRS, 42 avenue Gaspard Coriolis, 31057 Toulouse Cedex 1, France

12

13 **Key points**

14 We study the water masses dynamics of the western Mediterranean from a 20yr reanalysis using  
15 a  $\theta$ -S based algorithm of water masses fraction.

16 The method allows detecting anomalous events of deep water creation/destruction likely due to  
17 the assimilation process.

18 Results highlight the impact of deep water formation on the surface and intermediate regional  
19 circulation.

20

21 **Abstract**

22 We present an assessment of the water mass dynamics in a reanalysis of the Mediterranean Sea  
23 with a focus on the Western basin. We use a  $\theta$ -S based algorithm to compute the fractions of the  
24 main western Mediterranean water masses : Atlantic and modified Atlantic Waters (AW, mAW),  
25 Western and Levantine Intermediate Waters (WIW and LIW) and Western Mediterranean Deep  
26 Waters (WDW). The reanalysis retains the known mean characteristics of the water masses, their  
27 seasonal to interannual variability and main circulation patterns when compared with the  
28 literature. The imprints of winter mixing is particularly obvious with coherent variations of water  
29 mass volumes, mainly the yearly creation of WIW from mAW on northernmost shelves and of  
30 WMDW from all surface and intermediate layers during years of deep water formation. The  
31 results also highlight some unrealistic events of variability of the WMDW volume that are likely  
32 due to the data assimilation process. Re-computing the water mass volumes and transports  
33 without these altered years allowed to highlight the possible disruption of the large-scale  
34 barotropic cyclonic circulation in the Eastern Algerian basin in response to major DWF events  
35 over the Gulf of Lion. The reanalysis also shows an overtopping of WMDW in the Sardinia  
36 Channel in 2009 leading to a major backward flow of mAW from the Tyrrhenian to the Algero-  
37 Provençal basin. Both processes affects the circulations of AW and mAW over the whole  
38 western Mediterranean.

39

#### 40 **Plain Language Summary**

41 Defined as the large-scale oceanic circulation driven by surface heat and freshwater fluxes, the  
42 oceanic thermohaline circulation is a major player in the Earth's climate, as it distributes excess  
43 heat and carbon dioxide due to human activities into the deeper layers of the ocean over the long  
44 term. The Mediterranean Sea is unique in that it has its own thermohaline circulation due to its  
45 semi-enclosed configuration, a climate-driven water deficit (~ 1 m/year) balanced by a net inflow  
46 of Atlantic waters, and significant heat loss in winter leading to the formation of intermediate  
47 and bottom water masses. This thermohaline circulation has a time scale of around 100 years, 10  
48 times less than the global circulation, and has been shown to respond rapidly to the Northern  
49 Hemisphere climate variability. We have used a 20-year ocean reanalysis, i.e. a system that  
50 combines model and observations, to characterize and quantify the circulation of water masses in  
51 the western Mediterranean, from seasonal to interannual scales. Our study reveals that the main  
52 weakness of reanalysis lies in deep-water dynamics, whereas it has a marked imprint on surface  
53 and intermediate circulations. Understanding of the Mediterranean's future requires a better  
54 representation of its deep dynamics.

55

#### 56 **Abbreviations**

57 **Water Masses** : AW for Atlantic Water; LIW for Levantine Intermediate Water; mAW : for  
58 modified Atlantic Water; mIW for mixed Intermediate Water; TDW for Tyrrhenian Deep Water;  
59 TIW for Tyrrhenian Intermediate Water; WIW for Western Intermediate Water; WMDW for  
60 Western Mediterranean Deep Water

61 **Currents** : AC for Algerian Current; AE for Algerian Eddy; BC for Balearic Current; ECC for  
62 East Corsican Current; NC for Northern Current; SE for Sardinian Eddy; WCC for West  
63 Corsican Current

64 **Others** : DWF for Deep Water Formation; EMT for Eastern Mediterranean Transient; MEDRYS  
65 for MEDiterranean ReanalYSIS; MLD for Mixed Layer Depth; SLA for Sea Level Anomaly;  
66 WMT for Western Mediterranean Transition

67

#### 68 **1. Introduction**

69 The Mediterranean Sea has the unique particularity of having its own and well defined thermo-  
70 haline circulation, almost independent from the global one. This is due to its particular  
71 configuration : a semi-enclosed sea suffering a dry, windy and relatively warm regional climate  
72 that makes it a concentration basin where evaporation exceeds precipitation and run-offs (Nof,  
73 1979; Béthoux, 1980). This climate driven deficit of water (~0.5-1.0 m/year) is balanced by a net  
74 inflow through the Strait of Gibraltar between in-flowing AW and deeper out-flowing salty  
75 Mediterranean water (Nof, 1979; Millot, 1987; Béthoux & Gentili, 1999; Mariotti et al., 2002;  
76 Pellet et al., 2019). The incoming AW flows cyclonically in all the Mediterranean sub-basins  
77 toward the easternmost Levantine Basin and is continuously modified all along its path by  
78 mixing with saltier resident waters and air-sea exchanges. Simultaneously, severe heat loss and  
79 evaporation due to harsh atmospheric conditions in autumn and winter over the northern parts of  
80 the Mediterranean Sea causes convection to intermediate and deep layers (the deep water  
81 formation, DWF) in several areas and so to the recurrent formation of different intermediate and  
82 deep water masses. Those areas are mainly the Gulf of Lion for Western Mediterranean Deep

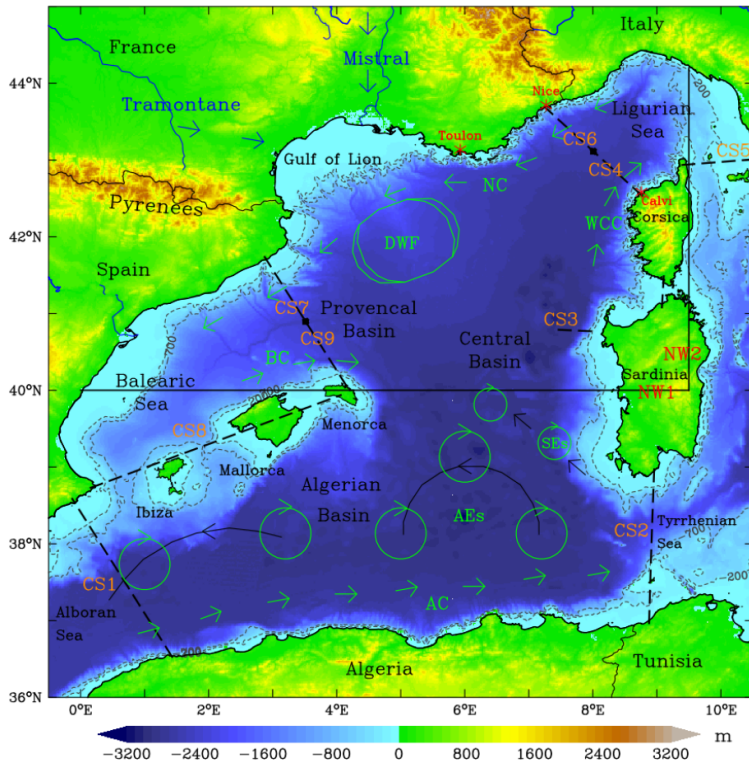
83 Water (WMDW), the Adriatic Sea and the Aegean Sea for the Eastern Mediterranean Deep Water  
84 (EMDW) and in the northern Levantine Basin for the very salty Levantine Intermediate Water  
85 (LIW). All those locally produced water masses mix and spread all together with the AW to set  
86 up and maintain the Mediterranean ThermoHaline Circulation (MTHC, [Robinson & Golnaraghi,  
87 1994](#); [Bergamasco & Malanotte-Rizzoli, 2010](#); [Waldman et al., 2018](#); [Pinardi et al., 2019](#)). The  
88 MTHC has a time scale of about 100 years (10 times less than the global Ocean one) and has  
89 been shown to quickly respond to Northern Hemisphere climate variability, be it during the last  
90 glacial period ([Cacho et al., 2000, 2001](#); [Incarbona et al., 2016](#); [Cortina-Guerra et al., 2021](#)) or  
91 more recently in the early 90's when an abrupt shift in the intermediate and deep part of the  
92 eastern MTHC, called the Eastern Mediterranean Transient (EMT), has affected the water  
93 masses in both parts of the Mediterranean for at least a decade ([Roether et al., 2007](#); [Bergamasco  
94 & Malanotte-Rizzoli, 2010](#); [Cardin et al., 2015](#); [Li & Tanhua, 2020](#); [Sisma-Ventura et al., 2021](#)).  
95 Subsequent to the propagation of the EMT signal in the western Mediterranean and after a lack  
96 of intermediate and deep convection in the early 00's, the sudden return of DWF events in 2005  
97 and after has led to a cooling and freshening of the intermediate waters associated with a  
98 warming and salting of the deep waters called the Western Mediterranean Transition (WMT,  
99 [Lopez-Jurado et al., 2005](#); [Schroeder et al., 2006, 2010, 2016](#); [Pineiro et al., 2019, 2021](#); [Amitai  
100 et al., 2021](#)).

101 All climate models predict in the Mediterranean an increase in rainfall variability and strong  
102 warming and drying ([Somot et al., 2008](#); [de Sherbinin et al., 2014](#); [IPCC AR6 WGI Full Report,  
103 2021](#)) while there is some evidence that the western DWF may collapse by mid-century due to  
104 increased stratification ([Somot et al., 2006](#); [Herrmann et al., 2008](#); [Parras-Berrocal et al., 2021](#)).  
105 Indeed, recent studies have shown the Mediterranean waters to have warmed at a rate four times  
106 larger than the global Ocean over the last decades ( $\sim 0.04^{\circ}\text{C}/\text{year}$  vs  $\sim 0.01^{\circ}\text{C}/\text{year}$ , [Bethoux et al.,  
107 1998](#); [Vargas-Yanez et al., 2008](#); [Nykjaer, 2009](#); [Bensoussan et al., 2019](#); [Pisano et al., 2020](#)),  
108 affecting all layers throughout the Mediterranean. These warning signals have led, over the last  
109 twenty years or so, to an unprecedented effort of sampling, modeling and analysis. However, an  
110 integrated and quantitative view of the MTHC able to improve the monitoring and future  
111 predictions of climate-induced changes still remains a challenge ([CIESM 2002](#); [Theocharis,  
112 2008](#); [Somot et al., 2008](#); [Fox-Kemper et al., 2019](#)). Here, we focus on the western  
113 Mediterranean which is known to be a four-layer system (surface, winter subsurface,  
114 intermediate and deep waters, [Juza et al., 2015](#)) and has six main water masses which are  
115 commonly and clearly identified in the literature : the AW and mAW in near surface layers (0-  
116 200m), the Western Intermediate Water (WIW,  $\sim 200\text{m}$ ) and LIW at intermediate depths (300-  
117 600m), the Tyrrhenian Deep Water (TDW, 500-1500m) and the WMDW at greater depths down  
118 to the bottom ([Wust, 1961](#); [Millot, 1987](#); [Manzella & La Violette, 1990](#); [Pinot et al., 1995](#); [Millot  
119 & Taupier-Letage, 2005](#); [Juza et al., 2013, 2019](#)).

120 The AW incoming from the strait of Gibraltar (0.6-1.0 Sv, [Soto-Navarro et al., 2010](#); [Peliz et al.,  
121 2013](#); [Skliris et al., 2018](#)) is the first input of the western MTHC and, except the Rhône and Ebro  
122 rivers plumes, is the lightest and freshest water of the western Mediterranean ( $S\sim 36.0$  at the  
123 Strait of Gibraltar). It flows along the North-African coast within the Algerian Current (AC, Fig.  
124 1), being spread and partially mixed northward in the Algerian basin by the Algerian Eddies  
125 (AEs, e.g. [Millot, 1990](#); [Puillat et al., 2002](#); [Testor et al., 2005b](#); [Escudier et al., 2016](#)) before  
126 flowing eastward toward the Tyrrhenian and through the strait of Sicily towards the Eastern  
127 Mediterranean ([Béranger et al., 2004](#); [Jebri et al., 2016](#)). MAW or mAW, for modified Atlantic  
128 Water is an acronym commonly used by many authors to designate the saltier AW due to its

129 ageing in the Mediterranean (e.g. Theocharis et al., 1993; Millot, 1999; Onken & Sellschopp,  
 130 2001; Puillat et al., 2002; Hassoun et al., 2015). It is sometimes also called old AW, (typical)  
 131 Mediterranean Water or Mediterranean Surface Water, (Millot et al. 2006; Millot, 2007, 2009).  
 132 Some others consider both the AW and mAW as a single entity (e.g. CIESM 2001, Millot &  
 133 Taupier-Letage, 2005; Béranger et al., 2005; Millot, 2013; Fedele et al., 2022). Both the AW and  
 134 mAW are restricted to the upper (0-200 m) layers but significantly differ in terms of salinity  
 135 values, the latter reaching two salinity units greater values (~38.2-38.4) for the saltier ones in the  
 136 Tyrrhenian and Ligurian Seas; hence the use of the appellation mAW for the present work. The  
 137 saltier mAW from the Tyrrhenian fuels the East Corsican Current (ECC) and joins with the West  
 138 Corsican Current (WCC) to feed the Northern Current (NC) that flows from the Ligurian to the  
 139 Balearic Sea (Fig. 1).

140



141

142 **Fig. 1.** Map of the western Mediterranean bathymetry and major circulations features. AC, BC,  
143 NC and WCC denote respectively the Algerian, Balearic, Northern and West Corsican currents.  
144 Large and small arrow circles denote the Algerian and Sardinian Eddies, respectively (AEs &  
145 SEs) while black arrows represent their paths. The oval shape locates the Deep Water Formation  
146 area. The CS sections locate where the transports of Table 2 have been calculated. The NW1  
147 section locates the section of Fig. 3, and with NW2, both define the NWMED domain as in  
148 [Somot et al. \(2018\)](#). Bathymetry data are from etopo1.nc ([NOAA National Geophysical Data](#)  
149 [Center. 2009](#))

150 The Levantine Intermediate Water (LIW) is the second major input of the western MHTC. LIW  
151 is produced in the Eastern Mediterranean by intermediate (~200-600 meters) convection in  
152 winter and is the saltier ( $S > 39$ ) of the Mediterranean ([Millot, 2013](#); [Ozer et al., 2017](#); [Kubin et](#)  
153 [al., 2019](#)). The LIW flows cyclonically along the continental slope at intermediate depths (200-  
154 600 meters) throughout the whole eastern basin and partly passes the strait of Sicily ([Millot,](#)  
155 [2013](#); [Ben Ismail et al., 2014](#)) to enter the western basin. When LIW enters the Tyrrhenian Sea, it  
156 mixes with resident deep waters (mostly WMDW) and forms the TDW ([Astraldi & Gasparini,](#)  
157 [1994](#); [Sparnocchia et al., 1999](#); [Gasparini et al., 2005](#)), but still keeping a pronounced salinity  
158 signature ( $S > 38.8$  between 300-600 meters). Both the LIW and TDW follow a counterclockwise  
159 circulation in the Tyrrhenian ([Falco et al., 2016](#); [de la Vara et al., 2019](#); [Iacono et al., 2021](#))  
160 before they leave through the Sardinia Channel to enter the Algero-Provençal basin where it flow  
161 northward along the western coasts of Sardinia and Corsica or are spreaded out westward in  
162 the central basin by the Sardinian Eddies (SEs) ([Rhein et al., 1999](#); [Testor et al., 2005a](#); [Bosse et](#)  
163 [al., 2015](#); [Send & Testor, 2017](#)).

164 The WIW is a winter cooled mAW due to cold and dry winds (Mistral and Tramontane) blowing  
165 over the shelf of the Gulf of Lion (GoL), the Provençal basin and the Ligurian Sea. Although not  
166 originally the saltiest of the mAW (~38.3), its cooling is sufficient to increase its potential  
167 density so as to make it sit between the warmer mAW and the deeper LIW at an intermediate  
168 depth of about 200-300 meters. It flows then mostly along the continental slope across the  
169 Balearic Sea and later through the Ibiza and Mallorca channels down to the Alboran Sea ([Salat &](#)  
170 [Font, 1987](#); [Puig et al., 2013](#); [Juza et al., 2019](#); [Vargas-Yanez et al., 2012, 2020](#)). Stronger winter  
171 wind forcing over the GoL and the Provençal basin regularly causes vertical convection through  
172 the WIW and LIW/TDW that can reach the seafloor in some years, leading then to the renewal of  
173 the WMDW ([MEDOC group, 1970](#); [Millot, 1999](#); [Schroeder et al., 2008ab](#); [Waldmann et al.,](#)  
174 [2016, 2017ab](#); [Testor et al., 2018](#), [Keller Jr. et al., 2022](#)). Intermediate convection during less  
175 severe winters produces a slightly less dense water that stands and stacks between the LIW and  
176 older deep water with thermohaline characteristics similar to the TDW. Constrained by the  
177 southward increasing bathymetry, the denser WMDW ( $\sigma_\theta > 29.10 \text{ kg m}^{-3}$ ) then spreads mostly  
178 southward across the whole Algero-Provençal basin up till the Alboran Sea. The WMDWs can  
179 sometimes pass through the Sardinia channel to enter the Tyrrhenian when exceptional DWF  
180 uplifts the older and lighter WMDW up to the strait sill, as following the WMT (e.g., [Beuviel et](#)  
181 [al., 2012](#); [Schroeder et al., 2016](#); [Li & Tanhua, 2020](#)).

182 To better understand the dynamics of these water masses, it is necessary to be able to follow their  
183 behavior and interactions, their entry or exit, their propagation and their mixing through the  
184 numerous mesoscale to sub-mesoscale eddies that are found throughout the NW Mediterranean.  
185 This challenge is hardly achievable with at-sea observations alone, while numerical modeling  
186 may not be free of biases and unrealistic trends due to uncertainties in forcing, initial conditions

187 and unresolved sub-grid processes. By combining, thanks to data assimilation systems, modeling  
188 and observations in a coherent physical framework, ocean reanalysis offers a good compromise,  
189 particularly for multi-decadal series which allow us to approach the climatology of the system  
190 and its inter-annual variability (Balsameda et al., 2015; Aznar et al., 2016). However, the  
191 reanalysis has its own weaknesses, mainly due to the assimilation process which, by forcing the  
192 model trajectory to converge towards independent observations, does not guarantee the pure  
193 conservation of heat and salt and can therefore alter the characteristics of the water masses.

194 This work is based on a reanalysis of the Mediterranean Sea, called MEDRYS1V2 (Hamon et  
195 al., 2016; Beuvier et al., 2016), with two main objectives : first, to assess the mean characteristics  
196 and distribution of water masses over the western Mediterranean as produced by the reanalysis,  
197 and second, to gain insight, characterize and quantify the circulation of these different water  
198 masses from seasonal to inter-annual time scales. We built a simple and efficient method to  
199 detect the water masses in the western Mediterranean and track their circulation and mixing over  
200 the twenty-year reanalysis (Section 2.2). The results are first analyzed using the mean  
201 thermohaline characteristics of each water mass to assess the robustness of the reanalysis in  
202 terms of water mass conservation. Climatological average of water mass volumes and transports  
203 are then assessed based on known circulation patterns (Section 3.1). In a second step, we analyze  
204 the time series of specific properties and volumes of each water mass (Section 3.2). In a third  
205 step, we focus the analysis on the DWF impact on surface dynamics at the climatological scale  
206 and by reference to the WMT (Section 3.3). We discuss the algorithm and the results, and  
207 conclude in Section 4.

208

## 209 2. Data & Methods

### 210 2.1. The MEDRYS1V2 Reanalysis

211 The study is based on the MEDRYS1V2 reanalysis which begins in October 1992 and ends in  
212 June 2013 with daily outputs (Hamon et al., 2016; Beuvier et al., 2016). These two decades  
213 allow us to compute quite good climatology of water mass volumes and transports and to  
214 observe several different episodes. MEDRYS1V2 is a configuration of the NEMO-MED12  
215 model (which has a spatial resolution of  $1/12^\circ$  and 75 z levels sharpened near the surface) that  
216 uses the SAM2 assimilation scheme (Lellouche et al., 2013). The simulation is forced by the  
217 atmospheric ALDERA dataset (Hamon et al. 2016), a downscaling of the ERA-Interim  
218 reanalysis (Dee et al., 2011) with the ALADIN-Climate regional climate model (Colin et al.,  
219 (2010) for the description of the version 5 of ALADIN-Climate used to produce the ALDERA  
220 dataset). Satellite SST, altimetry and *in situ* temperature-salinity ( $\theta$ -S) profiles are assimilated.  
221 SST data was assimilated at a resolution of  $1^\circ$  and comes from NOAA  $1/4^\circ$  gridded radiometer  
222 products (Reynolds et al., 2007) without trusting any observation within 50 km off the coasts.  
223 The along-track Sea Level Anomaly (SLA) AVISO product (1992-2013) is assimilated one  
224 every three points and combined with the Mediterranean MDT from Rio et al. (2011).  
225 Assimilated *in situ*  $\theta$ -S profiles from the CORA4 database (Cabanes et al., 2013) uses only one  
226 profile within  $0.1^\circ$  per day per platform. The reanalysis is initialized end of September 1992 with  
227 the state of a twin free run (same model configuration as MEDRYS1V2 but without data  
228 assimilation), which starts in October 1979. It takes about 9 months after its start for the  
229 reanalysis to achieve its spin up (see Hamon et al., 2016). Following results and validation hence  
230 do not take into account the first three seasons of the reanalysis (autumn 1992 to spring 1993).

## 231 2.2. The Detection Algorithm of Water Masses

232 Among the oldest tools of physical oceanography, the  $\theta$ -S diagram is classically used to analyze  
233 the mixing and distribution of water masses. It is based on the fact that the mixing of two water  
234 masses builds a straight line, allowing hence to determine the fraction of those for all sampled  
235 depth along this mixing line. The method is only a little more complicated for the mixing of three  
236 water masses considering that the sum of their fraction must equal unity. It becomes intractable  
237 for four water masses or more without considering at least another one conservative variable  
238 (e.g. Manca et al., 2006; Schroeder et al., 2008b; de Brauwere et al., 2007). Even in these cases,  
239 the other used variables should have to be sampled with the same spatio-temporal resolution that  
240 the  $\theta$ -S data, which is a hard to achieve task. Other methods can be found in the recent literature,  
241 such as clustering based methods (e.g. Kim et al., 1991; Cardin et Celio., 1997; Zhu et al., 2019)  
242 sometimes combined with EOF analysis on vertical profile of temperature and salinity (e.g.  
243 Hjelmervik & Hjelmervik, 2013; Bauch & Cherniavskaia, 2018; Gao et al., 2020), but were not  
244 considered given their high computing cost over a 20-y reanalysis.

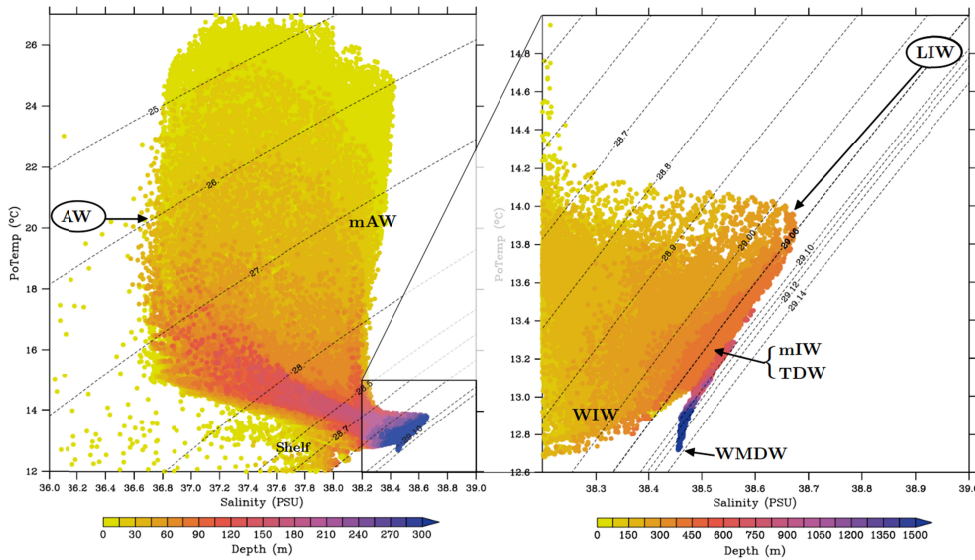
245 Indeed, we rather use the fact that, with the exception of transitory convection events, the vertical  
246 distributions of the different water masses are constrained by their relative buoyancy, i.e. are  
247 vertically ordered with increasing potential density. The water mass sorting algorithm was so-  
248 defined from the climatological (i.e. 20-y average)  $\theta$ -S diagram computed from the reanalysis  
249 (Fig. 2) assuming that, over the western Mediterranean, the water column can be partitioned in  
250 three main layers, each with different  $\theta$ -S mixing trends. AW and mAW ( $37 < S < 38.45$ ,  
251  $\theta > 13.5^\circ\text{C}$ ) are above 200-300m and can be easily distinguished from salinity alone. Temperature  
252 ranges seasonally from  $13^\circ\text{C}$  to more than  $25^\circ\text{C}$  in this upper layer and may only help in winter  
253 to identify WIW as cooled mAW ( $\theta < 13.5^\circ\text{C}$ ). Below 300m depth, a second mixing line reveals  
254 the transition toward a salinity maximum that marks the LIW core. Below this salinity  
255 maximum, the  $\theta$ -S diagram shows a third and almost linear mixing line from LIW to the  
256 WMDW, including TDW-like mixed intermediate waters. The water masses' sorting algorithm  
257 hence uses at first a partitioning of the water column based on potential density and, in a second  
258 step, ad hoc salinity and temperature dilution ratios along the three previously identified mixing  
259 lines. Using potential density based functions rather than fixed depths allows to dynamically  
260 adjust this partitioning of the water column all along the reanalysis. Likewise, dilution ratios are  
261 used afterward rather than net truncations that do not resolve water mass mixing and may  
262 generate spurious discontinuity effects in the vicinity of the threshold values used to discriminate  
263 the water masses. The main algorithm's hypotheses are as follows (computations' steps and  
264 equations are detailed in Appendix A).

265 At first, the partition of the water column is made with two functions defining the surface ( $f_{\text{surf}}$ )  
266 and deep ( $f_{\text{deep}}$ ) waters assuming the LIW marks the boundary between both (Appendix A.1).  
267 The surface layer is defined as all waters above the  $\sigma_\theta(\text{mAW}) = 28.964 \text{ kg m}^{-3}$  isopycnical  
268 ( $f_{\text{surf}} = 1$ ), assumed to mark the lower bound of the mAW core, and considering below a linear  
269 decrease of  $f_{\text{surf}}$  toward zero between  $\sigma_\theta(\text{mAW})$  and  $\sigma_\theta(\text{LIW}) = 29.061 \text{ kg m}^{-3}$ . The mAW's  
270 salinity (38.45) used to define  $\sigma_\theta(\text{mAW})$  is the maximum of time averaged sea surface salinity in  
271 the reanalysis (Fig. 2) and in observations in the Ligurian Sea (Marty & Chiavérini, 2010; Prieur  
272 et al., 2020). It is also the salinity minimum of WMDW (e.g., Puig et al., 2013; Houpert et al.,  
273 2016). The value used for  $\sigma_\theta(\text{LIW})$  is that of the original LIW in the eastern basin (taking  $S = 39$   
274 and  $\theta = 15^\circ\text{C}$ ) that is globally conserved in the reanalysis along the path of the LIW spreading  
275 (Fig. 2). The deep layer function is defined similarly assuming a linear increase from zero to



280 unity between LIW and WMDW, with a deeper bound  $\sigma_{\theta}(\text{WMDW})$  of  $29.11 \text{ kg m}^{-3}$  (assuming  
 281  $S=38.45$  and  $\theta=12.82^{\circ}\text{C}$ ) which is an often used lower bound for the WMDWs (e.g., Waldman et  
 282 al., 2017ab; Somot et al., 2018; Testor et al., 2018). This function directly gives the fraction of  
 283 WMDW ( $f_{\text{WMDW}}$ ) in the algorithm.

293 The LIW is first tagged using a salinity dilution ratio between 38.45 and 39 (Appendix A.2).  
 294 Note that as such, the LIW fraction ( $f_{\text{LIW}}$ ) is the residual of the original LIW being previously  
 295 mixed all along its path from the Levantine basin to the western basin. The AW is hence tagged  
 296 ( $f_{\text{AW}}$ ) using a salinity dilution ratio from  $S=36.0$ , i.e. the minimum salinity of inflowing AW  
 297 through the Strait of Gibraltar (see Table 1), to  $S=38.45$ , i.e. the maximum of time averaged sea  
 298 surface salinity in the reanalysis, coherently with the documented maximum value in the  
 299 Ligurian Sea (Prieur et al., 2020). In addition, we included a patch below  $S = 36.0$  to  
 300 discriminate fresh water ( $f_{\text{fresh}}$ ) of rivers, mainly the Rhône and Ebro Rivers, from the AW. This  
 301 freshwater fix produces false AW detections in the region of freshwater influence of both rivers,  
 302 where freshwater from both rivers would rather mix with resident mAW. However these false  
 303 AW detections are of very limited extent due to the sharpness of the salinity fronts on the edges  
 304 of the freshwater plumes and did not significantly affect volumes and transports estimates made  
 305 later on.



294

300 **Fig. 2.**  $\theta$ -S diagram colored by depth of the full average of the 20-years MEDRYS1V2  
 301 reanalysis, illustrating the several known water masses in the western Mediterranean basin  
 302 (except the Alboran and Tyrrhenian Seas' sub-basins as in Fig. 1). AW, mAW, WIW, LIW,  
 303 mIW, TDW, and WMDW denote respectively Atlantic Water, modified Atlantic Water, Western  
 304 Intermediate Water, Levantine Intermediate Water, mixed Intermediate Water, Tyrrhenian Deep  
 305 Water, and Western Mediterranean Deep Water. Shelf locates Gulf of Lion's shelf water.

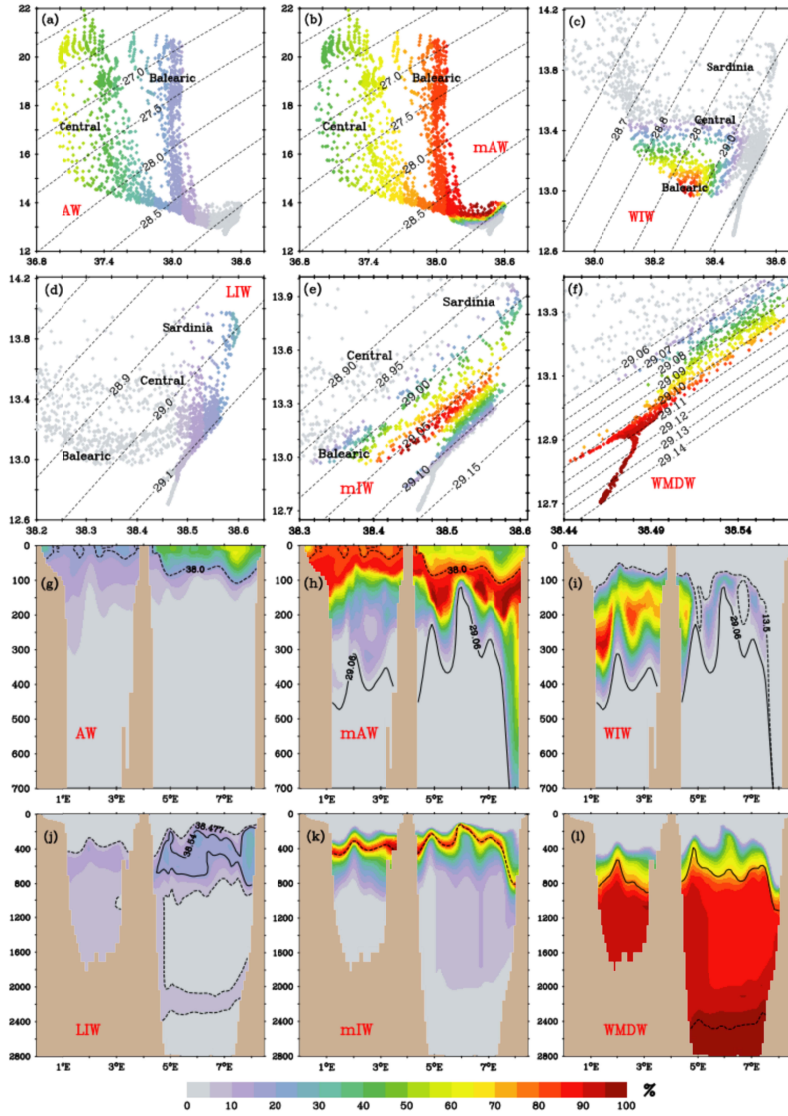
301

302 The mAW fraction ( $f_{\text{mAW}}$ ) is then defined as the complementary of AW, freshwater and LIW

302 flags in the upper layer, i.e.  $f_{mAW} = f_{surf} \cdot [1 - (f_{fresh} + f_{AW} + f_{LIW})]$ , with, in addition, a sub-  
303 partitioning of mAW to discriminate WIW using a temperature dilution ratio between 13°C and  
304 13.5°C when  $\theta$  is lower than 13.5°C (Appendix A.3). This WIW labeling is an intermediate  
305 method between a fixed range detection and the geometry-based method of [Juza et al. \(2019\)](#). At  
306 last, we define a pool of intermediate mixed waters, called mIW, as the complementary of the  
307 sum of all previously computed flags, i.e.  $f_{mIW} = 1 - (f_{fresh} + f_{AW} + f_{mAW} + f_{WIW} + f_{LIW} + f_{WMDW})$ , that  
308 may include TDW as well as all partially mixed waters of similar thermohaline characteristics  
309 produced during intermediate or uncomplete DWF events over the GoL. None of those  
310 intermediate water masses is able to generate an inflection point on the  $\theta$ -S diagram that may  
311 help to unambiguously discriminate them.

312 Fig. 3 shows an illustrative example of the  $\theta$ -S-flags diagrams and corresponding vertical  
313 distribution of the so-tagged water masses for a zonal section at 40°N in the late-spring of 2009.  
314 Higher flag values properly match the known  $\theta$ -S ranges of each water mass, mixing trends  
315 between each and vertical distributions. Waters above  $\sigma_\theta = 29.0 \text{ kg m}^{-3}$  are mainly AW and mAW,  
316 showing a zonal transition between the Balearic Sea, where mAW are mostly found, and the  
317 central area where the signature of AW is slightly more pronounced. Both are tagged in the  
318 upper 300 m and well above the LIW. WIW is located between mAW and LIW and  
319 preferentially in the Balearic Sea in a vein of low temperature (13-13.3°C) and moderate salinity  
320 (38.1 to 38.4). LIW is tagged between 200 and 800m depth, preferentially on the Sardinian coast,  
321 but also showing some traces at great depths (2000-2200 m) likely resulting from a previous to  
322 2009 convection event ([Pineiro et al., 2021](#)). The WMDW is labeled at depth ( $f_{WMDW}$  greater  
323 than 75% below 800m) and mainly below the 29.10  $\text{kg m}^{-3}$  isopycnical. The mIW is tagged on  
324 the WIW/LIW and LIW/WMDW mixing lines, centered around the 29.06  $\text{kg m}^{-3}$  isopycnical  
325 with a larger extent at depth (800 m).

326



328 **Fig. 3.**  $\theta$ -S diagrams (a-f) and (g-l) corresponding vertical cross-sections of the water mass ratios  
 329 (%) along 40°N (NW1 section on Fig. 1) for 28 May 2009. Some critical isolines are shown on  
 330 vertical section panels as : dotted line for the 38.00 isohaline (g-h); solid line for the 29.06 kg m<sup>-3</sup>  
 331 isopycnal (h) ; dotted line for the 13.5 °C isotherm and solid line for the 29.06 kg m<sup>-3</sup> isopycnal  
 332 (i) ; solid and dotted lines for the 38.54 and 38.477 isohalines, respectively (j) ; dotted line for  
 333 the 29.06 kg m<sup>-3</sup> isopycnal (k) ; solid line and dotted lines for the 29.10 kg m<sup>-3</sup> and 29.13 kg  
 334 m<sup>-3</sup> isopycnals (l), respectively. Balearic, Central and Sardinia locate the data of the Balearic Sea,  
 335 the Central basin and the shelf's slope of Sardinia.

336 With the water masses marked in this way, several diagnostic quantities were calculated (see  
 337 Appendix B for details of the calculations), first to check the robustness and efficiency of the  
 338 algorithm over all the reanalysis, and second to extract the distributions and transports of each  
 339 water mass. Based on the fact that the sum of the water mass fractions is always constrained to  
 340 unity, these are first used as weighting factors to extract the volume-averaged thermohaline  
 341 characteristics of each water mass over the study area. The core characteristics of each water  
 342 mass are calculated similarly but using only the local maximum within the water column of the  
 343 corresponding flag. We also calculated the depth range occupied by each water mass by  
 344 averaging the minimum and maximum depths of each water column where the corresponding  
 345 fraction is greater than 0.05 (5%). Still based on a sum of fractions equal to unity, the water mass  
 346 fractions are then used to partition the volumes and advective fluxes for each grid cell, allowing  
 347 the calculation of water mass-specific volumes and transports from the water column level (by  
 348 depth integration) to the regional scale (by meridional and zonal integration).

349

### 350 3. Results

#### 351 3.1. Average Thermohaline Characteristics, Volumes and Circulations of the Water Masses

352 This section presents climatological averages (i.e. 20-year averages) of the thermohaline  
 353 characteristics, volumes and transports of each water mass as labeled by the algorithm. The  
 354 average characteristics ( $\theta$ , S,  $\sigma_\theta$ , z) are first given in Table 1 for comparison with known  
 355 literature values (references therein the table). The calculated specific volumes and transports are  
 356 presented in Figure 4. Reported per square meter for each model grid point, the estimated  
 357 volumes (in m<sup>3</sup>) also correspond to the thickness of the water mass layer (in meters). Table 2  
 358 gives transport values computed at selected sections (see Fig. 1) to facilitate the comparisons  
 359 with known transports of the major currents in the literature.

360 The mean salinity of the AW is estimated to be  $37.565 \pm 0.071$  (average  $\pm$  one standard  
 361 deviation), slightly lower but more variable within the core of the water mass computed with the  
 362 maximum flag value ( $37.289 \pm 0.123$ ). These values are about 1.5 units higher than those of the  
 363 AW entering through the Strait of Gibraltar (S~36) and reflect the progressive mixing with the  
 364 Mediterranean saltier waters in the Alboran gyre system and further east in the AC instabilities  
 365 and associated AEs. The AW mean temperature is ca  $15.954 \pm 1.32^\circ\text{C}$ , close to the mean values  
 366 for the inflowing AW, with a standard deviation of 1.32-1.85 °C (core and whole estimates,  
 367 respectively) that accounts for the seasonal cycle of surface layers in the area. As such, the AW  
 368 is the lightest water mass, showing average potential density values less than  $28.0 \text{ kg m}^{-3}$ , a  
 369 maximum depth of  $135 \pm 16 \text{ m}$  and a core's mean depth close to the surface ( $22 \pm 9 \text{ m}$ ).

370

371 **Table 1.** Historical and computed (20y and spatial average, standard deviation in brackets) values of  
 372 potential temperature, salinity, potential density anomaly and depth location of the water masses in the  
 373 western Mediterranean. The locations of historical studies are indicated with Lig., Bal, Prov., Lev, Alg.-  
 374 Prov and Tyr. denoting respectively the the Ligurian and Balearic Seas, the Provençal area, Levantine,  
 375 Algero-Provençal basin and Tyrrhenian Sea.

376

Water Mass	$\theta$ (°C)	PSAL	$\sigma_\theta$ (kg.m <sup>-3</sup> )	Depth range (m)	Location & period	References	
AW	>15	36.0-36.4	<27	<200	Gibraltar, 1955-2007	Bryden et al., 1994; Millot, 2007, 2009; Carracedo et al., 2014	
	14-25	37.5-37.8	~25	0-150	Bal. Sea & Alg.-Pro. 1996-2020	Vargas-Yanez et al., 2020; Barral et al., 2021; Fedele et al., 2022	
	<b>Full</b>	15.954 (1.32)	37.565 (0.071)	27.702 (0.338)	min 0 (0) ave 34 (2) max 135 (16)	Alg.-Pro. 1993-2013	This study
	<b>Core</b>	16.907 (1.849)	37.289 (0.123)	27.273 (0.507)	ave 22 (9)		
mAW	>13	38.0-38.5	27.5-29	0-300	Lig. Sea & Prov. area 1980-2018	Marty & Chiverini, 2010; Puig et al., 2013; Prieur et al., 2020	
	<b>Full</b>	14.508 (0.605)	38.107 (0.04)	28.462 (0.147)	min 0 (0) ave 63 (8) max 253 (36)	Alg.-Pro. 1993-2013	This study
	<b>Core</b>	13.798 (0.355)	38.302 (0.042)	28.779 (0.09)	ave 114 (27)		
WIW	11.5-13.5	37.7-38.6	28.9-29.1	100-300	Bal & Pro 1983-2019	Salat & Font, 1987; Puig et al., 2013; Juza et al., 2019; Vargas-Yanez et al., 2012, 2020	
	<b>Full</b>	13.204 (0.084)	38.356 (0.05)	28.953 (0.024)	min 131 (29) ave 151 (51) max 257 (33)	Alg.-Pro. 1993-2013	This study
	<b>Core</b>	13.217 (0.074)	38.358 (0.038)	28.953 (0.016)	ave 164 (32)		
LIW	$\geq 15$	39-39.2	29.06	200-500	Lev. basin 1978-2017	Millot, 2013; Ozer et al., 2017; Kubin et al., 2019	
	13.1-13.9	38.5-38.7	29.05-29.1	200-800	Alg.-Pro. 2000-2019	Puillat et al., 2006; Bosse et al., 2015; Mallil et al., 2021; Fedele et al., 2022	
	<b>Full</b>	13.151 (0.046)	38.518 (0.009)	29.09 (0.009)	min 273 (28) ave 703 (96) max 1269 (401)	Alg.-Pro. 1993-2013	This study
	<b>Core</b>	13.385 (0.053)	38.564 (0.017)	29.077 (0.011)	ave 425 (40)		
TDW	12.8-13.7	38.43-38.7	>29.09	>700	Tyr. Sea 1987-2018	Fuda et al., 2002; Buffett et al., 2017; Napolitano et al., 2019; Li & Tanhua, 2020	
	>12.86	38.46-38.56		600-1900	Alg.-Pro. 1997-2002	Rhein et al., 1999; Send & Testor, 2017; Ben Ismail et al., 2021	
miW	<b>Full</b>	13.149 (0.086)	38.497 (0.018)	29.075 (0.006)	min 205 (26) ave 525 (138) max 1344 (402)	Alg.-Pro. 1993-2013	This study
	<b>Core</b>	13.309 (0.054)	38.518 (0.014)	29.057 (0.001)	ave 325 (51)		
WMDW	12.7-13	38.4-38.5	>29.1	>1500	Alg.-Pro. 1990-2014	Millot, 1999; Fuda et al., 2000; Puig et al., 2013; Schroeder et al., 2006, 2016; Knoll et al., 2017	
	<b>Full</b>	12.910 (0.032)	38.476 (0.013)	29.108 (0.007)	min 360 (56) ave 1382 (85) max 2246 (21)	Alg.-Pro. 1993-2013	This study
	<b>Core</b>	12.783 (0.026)	38.461 (0.010)	29.122 (0.009)	ave 2192 (129)		

377

378 The AW is mainly detected (Fig. 4a) in the Algerian basin, within the AC and the AEs spreading

379 area toward 40-41°N with some intrusions in the Balearic Sea through the Ibiza Channel (see  
380 Millot, 1987; Pinot et al., 1995). The AW transport exiting the Alboran Sea is estimated to  $0.58 \pm$   
381  $0.31$  Sv (CS1 in Table 2), from which a little part passes the channel of Ibiza ( $0.08 \pm 0.15$  Sv,  
382 CS8) while the largest part flows eastward through the Sardinia Channel toward the Tyrrhenian  
383 ( $0.37 \pm 0.25$  Sv, CS2). In both cases, the standard deviations reflect a high variability ( $0.15$ - $0.25$   
384 Sv) likely due to the mesoscale activity that prevails in the AC and AEs. There is no significant  
385 AW transport north to 41°N, i.e. only very low values (lower than  $2 \times 10^{-3}$  Sv) due to traces of  
386 tagged AW ( $f_{AW}$  under 5%), left by the use of a linear salinity dilution ratio between AW and  
387 mAW in the algorithm rather than a fixed threshold. The imbalance in AW transport between the  
388 inflow from Alboran and the outflow through the Sardinia Channel is compensated by a  
389 significant eastward flow of mAW through the Sardinia Channel (see below), highlighting the  
390 mixing of AW with the resident Mediterranean waters in the instabilities of the AC and the AEs.

391 The labeled mAWs show higher mean salinities of 38.107 in the whole and 38.302 in the core,  
392 but in both cases with a low standard deviation (ca 0.04). The mean temperatures are lower than  
393 for the AWs ( $13.798^\circ\text{C}$  and  $14.508^\circ\text{C}$  for the core and the whole, respectively), and less variable  
394 (standard deviation less than  $0.355$ - $0.605^\circ\text{C}$ ), mainly due to their more northerly and deeper  
395 distribution (see Fig. 3). Mean densities are therefore higher ( $28.462$ - $28.779$   $\text{kg m}^{-3}$ ), as are the  
396 whole's maximum ( $253 \pm 36$  m) or the core's mean ( $114 \pm 27$  m) depths. The algorithm labels an  
397 eastward, increasing volume of mAW in the Algerian basin in response to the salinity increase  
398 along the path of AW toward the Tyrrhenian and, coherently, a higher volume of mAW in the  
399 Tyrrhenian. While the transports through the Sardinia Channel show both eastward and  
400 westward flows for the mAW, the net balance is eastward ( $0.35 \pm 0.47$  Sv) and compensates for  
401 the imbalance of AW transport between the Alboran exit and the Sardinia Channel. In the  
402 northern part of the basin (North of 40°N), the mAW is tagged along the shelf's slope, showing  
403 the well-known cyclonic circulation from the West Sardinia to the Balearic Sea with an offshore  
404 undulating return flow between Mallorca to Sardinia around 40°N. The lower amount of mAW  
405 in the center of this gyre is consistent with the well-known isopycnal doming in the wintertime  
406 convective areas (e.g., Prieur et al., 2020). The mean transport of mAW increases from  $0.12 \pm$   
407  $0.36$  Sv along the shelf's slope of West Sardinia (CS3), to  $0.49 \pm 0.41$  Sv in the WCC off Calvi  
408 (CS4). Then, being reinforced by the ECC from the Tyrrhenian ( $+0.29 \pm 0.31$  Sv, CS5), the  
409 mAW flow finally reaches  $0.72 \pm 0.43$  Sv in the NC off Nice (CS6), but clearly decreases off the  
410 Gulf of Lion before entering the Balearic Sea ( $0.32 \pm 0.50$  Sv, CS7). Part of this decrease comes  
411 from the long-time average effect of winter times when mAW temporarily vanishes due to their  
412 conversion in new WIW during the coldest months and ultimately in WMDW during deep  
413 convection events.

414 The average thermohaline characteristics of WIW are close to those of mAW, showing only a  
415 slightly higher salinity ( $38.356 \pm 0.05$ ) and, as expected, a lower temperature ( $13.204 \pm$   
416  $0.084^\circ\text{C}$ ) with no significant difference between the full and core estimates. The low standard  
417 deviations of the mean temperatures of the WIWs are due to the narrow range of temperatures  
418 that defines them and their short period of contact with the ocean-atmosphere interface. The  
419 WIW is generally defined as colder than  $13^\circ\text{C}$ , but the 20-y average uses all days of the year and  
420 not only winter days when the recent WIW is at its coldest. In addition, Juza et al. (2019) and  
421 Vargas-Yanez et al. (2020) have shown a warming trend in the WIW of  $0.5^\circ\text{C}$  over the last  
422 decade. The corresponding mean potential density of the WIW ( $28.953$   $\text{kg m}^{-3}$ ) is slightly higher  
423 than that of the mAW's core ( $28.779$   $\text{kg m}^{-3}$ ), leading to a depth range ( $131 \pm 29$  to  $257 \pm 33$  m)  
424 that lies between the mAW and LIW cores (114 and 425 m). The average total volume of WIW

425 over the Algero-Provençal domain is  $17.3 \times 10^3 \text{ km}^3$ , distributed mainly along the Gulf of Lion  
 426 shelf-slope and over most of the catalano-balearic area in agreement with estimates of [Juza et al.](#)  
 427 (2013, 2019). The WIW average transport off the Catalan coast is estimated to be  $0.20 \pm 0.32 \text{ Sv}$ ,  
 428 part of which escapes from the Balearic Sea through the BC ( $0.11 \pm 0.17 \text{ Sv}$ ) and a lesser amount  
 429 through the channels of Ibiza and Mallorca toward the Alboran Sea ( $0.08 \pm 0.12 \text{ Sv}$ ). These  
 430 estimates are consistent with those of [Juza et al. \(2013\)](#), although they use a much higher  
 431 resolution model ( $1/40^\circ$ ) and a shorter period. Finally, as the algorithm considers WIW as cold  
 432 mAW, WIWs' volume and transport mirror the decrease of mAW ones from the Gulf of Lion to  
 433 the Balearic Sea. Adding both transports compensates for the loss of mAW between Nice and the  
 434 Balearic Sea.

435 **Table 2.** Twenty year averaged water masses transports (Sv) and standard deviations (in  
 436 brackets) computed across the transects shown Fig. 1. The ones for the Alboran Sea and the  
 437 Sardinia Channel are positive eastward ; all others are positive northward. Transports between  
 438 Corsica and Sardinia are not shown (lower than  $10^{-5} \text{ Sv}$ ).

439

	AW	mAW	WIW	LIW	mIW	WMDW
CS1: Alboran Sea	0.579 (0.306)	0.133 (0.342)	-0.086 (0.088)	-0.060 (0.050)	-0.324 (0.226)	-0.198 (0.576)
CS2: South of Sardinia	0.373 (0.254)	0.345 (0.472)	0.0 (0.01)	-0.194 (0.160)	-0.088 (0.148)	-0.065 (0.462)
CS3: WCC off Sardinia	0.018 (0.062)	0.171 (0.368)	0.0 (0.062)	-0.009 (0.112)	-0.136 (0.405)	-0.246 (0.748)
CS4: WCC off Calvi	0.062 (0.048)	0.487 (0.412)	0.09 (0.141)	0.056 (0.159)	0.348 (0.892)	0.142 (0.408)
CS5: East of Corsica	0.034 (0.044)	0.294 (0.312)	0.006 (0.037)	0.010 (0.015)	0.005 (0.014)	0.000 (0.001)
CS6: NC off Nice	-0.075 (0.05)	-0.72 (0.43)	-0.142 (0.219)	-0.068 (0.165)	-0.351 (0.890)	-0.163 (0.401)
CS7: NC off Pyrenees	-0.044 (0.093)	-0.323 (0.497)	-0.204 (0.325)	-0.047 (0.082)	-0.295 (0.372)	-0.387 (0.842)
CS8: Balearic channels	0.082 (0.154)	-0.025 (0.351)	-0.083 (0.115)	-0.011 (0.023)	-0.139 (0.206)	-0.063 (0.154)
CS9: BC off Menorca	0.095 (0.101)	0.310 (0.377)	0.111 (0.170)	0.027 (0.077)	0.143 (0.337)	0.374 (0.858)

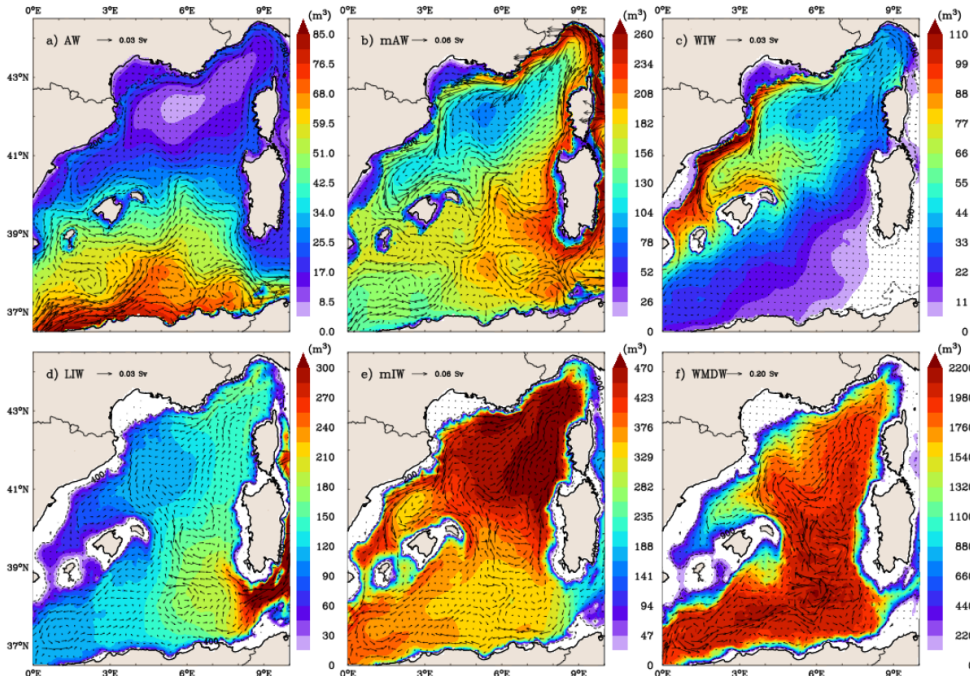
440

441 The algorithm gives the LIW mean salinity as  $38.518 \pm 0.009$ , with only a slightly higher value  
 442 for the core ( $38.564 \pm 0.017$ ). These low values are consistent with a -0.4 PSU loss due to the  
 443 LIW dilution from the Levantine to the Western basin (e.g. [Millot et al., 2013](#); [Schroeder et al.,](#)  
 444 [2020](#)). Its relatively low mean temperatures ( $13.151 \text{ }^\circ\text{C}$ ) can be interpreted in the same way,  
 445 while less marked within the warmer LIW core ( $13.385 \text{ }^\circ\text{C}$ ). Note that the estimated global LIW  
 446 characteristics also include the older LIW which is distributed over all depths, especially during  
 447 deep convection events, leading to traces of LIW in the deeper layers (see Fig. 3). This bias also  
 448 affects the calculated depth range ( $273 \pm 28\text{m}$  to  $1269 \pm 401\text{m}$ ) and overall potential density  
 449 ( $29.09 \text{ kg m}^{-3}$ ). However, the core calculation better matches the main LIW vein flowing along  
 450 western Sardinia at about 400 meters depth in [Bosse et al. \(2015\)](#), with salinities over 38.56,  
 451 temperatures over  $13.39 \text{ }^\circ\text{C}$  and a potential density of  $29.075 \text{ kg m}^{-3}$ . This latter value is slightly  
 452 higher than the one used in the algorithm ( $29.06 \text{ kg m}^{-3}$ ) as a specific characteristic of the  
 453 original LIW, but closer to the one usually found in the northwestern Mediterranean (e.g., [Puig et](#)  
 454 [al., 2013](#); [Schroeder et al., 2020](#)). The largest LIW volume is detected over the Sardinia Channel,

455 given the proximity of the Tyrrhenian where LIW is known to accumulate (e.g., [Sammari et al.,](#)  
456 [1999](#)). LIW volumes decrease rapidly westwards with lowest (or even null) volumes over the  
457 shallowest areas, i.e. the GoL shelf, the East of Corsica and the Balearic Islands, ensuring that  
458 the algorithm effectively identifies them as intermediate waters. The associated transports show a  
459 turbulent eddy-like propagation between southern Sardinia and the Balearic archipelago, and a  
460 weak cyclonic flow (0.01–0.07 Sv) along the shelf slope over most of the western basin, except  
461 for an offshore separation of the main flow (0.027 Sv) at the entrance to the Balearic Sea  
462 somewhat linked toward northern Corsica. This cyclonic flow along the shelf slope is consistent  
463 with historical finding about the LIW behavior (e.g. [Millot & Taupier-Letage, 2005](#)) and the  
464 eddy-like flow in the central area would reflect the average effect of the SEs' drift (e.g. [Testor et](#)  
465 [al., 2005a](#); [Bosse et al., 2015](#)). The absence of a significant LIW flow along Corsica north of  
466 41°N is coherent with the detachment of the “Suddies” northwest of Sardinia in [Bosse et al.](#)  
467 [\(2015\)](#) while the offshore LIW flow midway between Menorca and Corsica follows the mAW  
468 and WIW recirculations in the northern gyre has, to our knowledge, never been suggested nor  
469 demonstrated.

470 The mean density of the tagged WMDW is close to the usual definition value of  $29.10 \text{ kg m}^{-3}$ ,  
471 both for the total ( $29.108 \pm 0.007 \text{ kg m}^{-3}$ ) and the core estimates ( $29.122 \pm 0.009 \text{ kg m}^{-3}$ ). The  
472 WMDW is detected at a depth greater than  $360 \pm 56\text{m}$  (fractions greater than 5%) with a  
473 maximum depth ( $2246 \pm 21\text{m}$ ) and a core depth ( $2192 \pm 129\text{m}$ ) that closely follows the average  
474 bottom depth of the area. Its density-based tagging gives mean salinities of 38.476 (entire) and  
475 38.461 (core) with small standard deviations (0.010–0.013), close to the usually observed range  
476 (see Table 1). The mean temperatures are also close to the usual estimates, being  $12.783 \pm 0.032$   
477 and  $12.910 \pm 0.026 \text{ }^\circ\text{C}$  for the ensemble and core, respectively. Due to its greater vertical extent,  
478 the WMDW volumes are of a higher order than other water mass volumes, and closely follows  
479 the bathymetry of the basin, the higher values being in the southern deepest area. It could be  
480 surprising that the highest volume is not found in the DWF area, but this reflects the rapid  
481 (within a few months e.g. [Beuvier et al., 2012](#)) southward spreading of newly formed WMDWs  
482 following the general increase in bathymetry to the south. The WMDW transports reveal a  
483 turbulent eddy-like circulation between southern Sardinia and the Balearic Archipelago and two  
484 cyclonic circulations over, respectively, the south-western basin between the Balearic  
485 Archipelago and North Africa and the north-western Liguro-Provençal area. The associated  
486 transports (Fig. 4 and Table 2) are of the same order as those of mAW and mIW, the greater  
487 depth range of the WMDW (thousands of meters) compensating for the lower velocities (below 5  
488 cm/s) that prevail in the deeper layers.





489

490 **Fig. 4.** Climatology of model grid water mass volumes ( $\text{m}^3$ ) and transports (Sv) averaged over  
 491 the 1993-2013 period: Atlantic Water (a), modified Atlantic Water (b), Western Intermediate  
 492 Water (c), Levantine Intermediate Water (e), mixed Intermediate Water (e) and Western  
 493 Mediterranean Deep Water (f). A scale arrow for transport values is shown on each panel.

494

495 As the mIW flag adds up what is left of all the other water masses, it is not a defined water mass  
 496 but a residual mixture likely including TDW and more generally all intermediate waters from the  
 497 eastern basin that may have passed the Sicily and Sardinia Channel (e.g. Millot et al., 2013,  
 498 Schroeder et al., 2020), as well as those produced in the Northwestern provençal area due  
 499 intermediate convection events. As such, its average characteristics cannot be objectively  
 500 compared with the literature, but have to be coherent with the surrounding water masses. The  
 501 mean salinities of the mIW ( $38.497 \pm 0.018$  for the whole and  $38.518 \pm 0.014$  for the core) are  
 502 midway between those of the LIW and the WMDW, thus well on the mixing line between them.  
 503 In contrast, the mean temperatures ( $13.149 \pm 0.086$  and  $13.309 \pm 0.054$ ) are slightly warmer than  
 504 the average between LIW and WMDW which is more like  $13^\circ\text{C}$ . The average potential density  
 505 of the whole mIW is  $29.075 \text{ kg m}^{-3}$ , close to that of LIW, while that of the core is slightly lower  
 506 at  $29.057 \text{ kg m}^{-3}$ . This reflects the fact that mIW is also labeled on a significant part of the upper  
 507 intermediate layers, i.e. between the mAW/WIW and the LIW and not only in the deep layers  
 508 below the LIW (see Fig. 3). The range of calculated mIW depths is consistent with these  
 509 findings, showing a minimum of  $205 \pm 26 \text{ m}$ , close to the maximum depths of the mAW and  
 510 WIW, a core depth of  $325 \pm 50 \text{ m}$  and a maximum depth of  $1344 \pm 402 \text{ m}$  close to the LIW's  
 511 one. The mIW volumes are the second highest, twice as high as mAW or WIW but five times

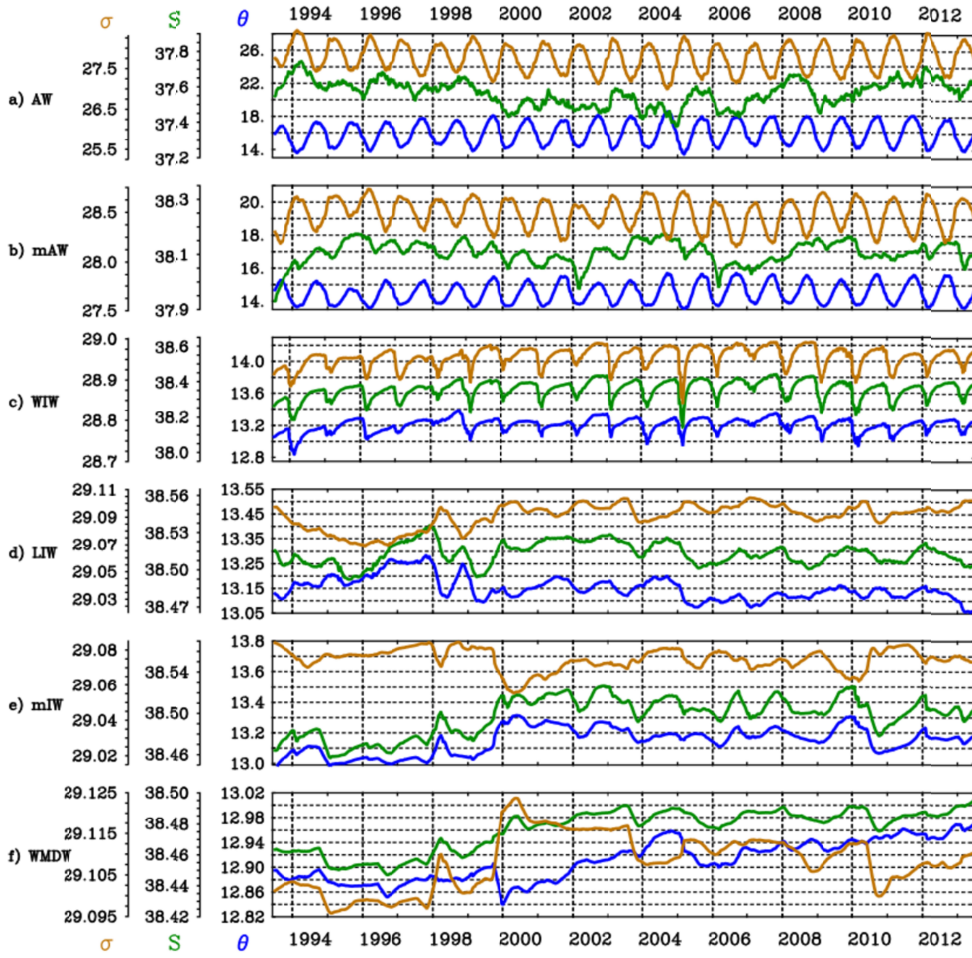
512 lower than WMDW, and have a general distribution opposite to WMDW with higher values in  
513 the most north-eastern part of the area. The circulation patterns are similar but less pronounced  
514 than those of the WMDW, except over the Balearic Sea where they rather follow those of the  
515 mAW/WIW. The corresponding transport values are most often intermediate between mAW and  
516 WIW over the northern part of the basin, ranging from 0.1-0.3 Sv (Table 2), but predominate  
517 through and south of the Balearic islands.

### 518 3.2. Time Series of Thermohaline Characteristics and Volumes of the Water Masses

519 Given the coherent long term mean of the water mass characteristics, volumes and circulations  
520 described in the previous section, we now look for their variability over the whole 20-y of the  
521 reanalysis. To do so, we present the time series of the characteristics (Fig. 5) and volumes (Fig.  
522 6) of the water masses, with the corresponding maximum mixed layer depth (MLD) and DWF  
523 area extent (Fig. 6). The temperature variability on the surface water masses (AW, mAW) is first  
524 driven by the seasonal radiative cycles and enforced by strongest winds in winter time, i.e.  
525 classically, a cooling in autumn and winter and a warming in spring and summer. The mAW  
526 salinity shows a weaker (and even sometimes unclear) seasonal variability while the AW salinity  
527 does not show any seasonal cycles, coherently with the almost constant flow of AW through the  
528 strait of Gibraltar. This nearly constant AW flow also explains the low variability of the AW  
529 volume (Fig. 6). The seasonal variability of densities of the water masses then mainly depends  
530 on their temperature. By contrast, the mAW volumes exhibit a marked seasonal cycle with  
531 winter drops that mirror the increases of WIW volumes, materializing the conversion of mAW to  
532 WIW in winter time. Coherently, all WIWs' thermohaline characteristics show strong seasonal  
533 variations (Fig. 5c) with minimum temperature and salinity in winter (ca 13.0°C and 38.25) and  
534 increasing values from spring to summer due to its mixing with surrounding warmer water  
535 masses from below (the LIW) and from above (AW and mAW) given the summertime  
536 stratification of the surface layers. As such, the WIWs' volumes range from  $10 \times 10^3 \text{ km}^3$  in  
537 summer to  $28 \times 10^3 \text{ km}^3$  in winter close to the range estimated by [Juza et al. \(2019\)](#) for 2011-  
538 2013 ( $10 \times 10^3 - 50.10^3 \text{ km}^3$ ). Note that the most severe drops in mAW volumes, which exceed  
539 the increase in WIW, occur during the DWF years (e.g., 1999 and 2005), affecting as well the  
540 WIW thermohaline characteristics.

541 On longer time scales, the mAW and AW salinities' time series show periods of alternating  
542 increase and decrease, but of limited amplitude (0.15) and not concomitant in time. We also note  
543 that maxima of mAW's volume tend to increase during the periods with several years of low or  
544 no convection (1996-1998, 2001-2002, 2007-2009) and, conversely, stay nearly constant during  
545 periods of consecutive medium to strong convection (1999-2000, 2003-2006, 2010-2013). This  
546 suggests that the destruction of the mAW by DWF in the northern sub-basin is generally  
547 balanced later in the year by its production by mesoscale horizontal mixing in the AEs' while  
548 several consecutive years of low or no convection may favor the accumulation of mAW over the  
549 whole basin. However, there are some exceptions to this global rule in 2001-2002 (stagnating  
550 mAW maximum volume instead of an increase) and in 2009 (increasing summer's mAW  
551 maximum volume instead of a stagnation). In the first case, it seems that from summer to  
552 summer, the period of no or low convection was too short to significantly affect the mAW  
553 volume. The 2009 year is an exceptional case that will find a more rational explanation later  
554 (Section 3.3). Lastly, the AW volumes exhibit similar, but low, drops during years of medium to  
555 strong convection followed by relaxing periods during low or no convection years. This  
556 similarity between the AW and mAW pluri-annual variability is likely due to the use of a salinity

561 ratio in the algorithm that retains a small amount of AW over the northern part of the basin. As  
 562 the years of medium to strong convection are more frequent during the second half of the  
 563 reanalysis, this leads to a general tendency of decreasing AW amount (-25 %) over the whole  
 564 area.



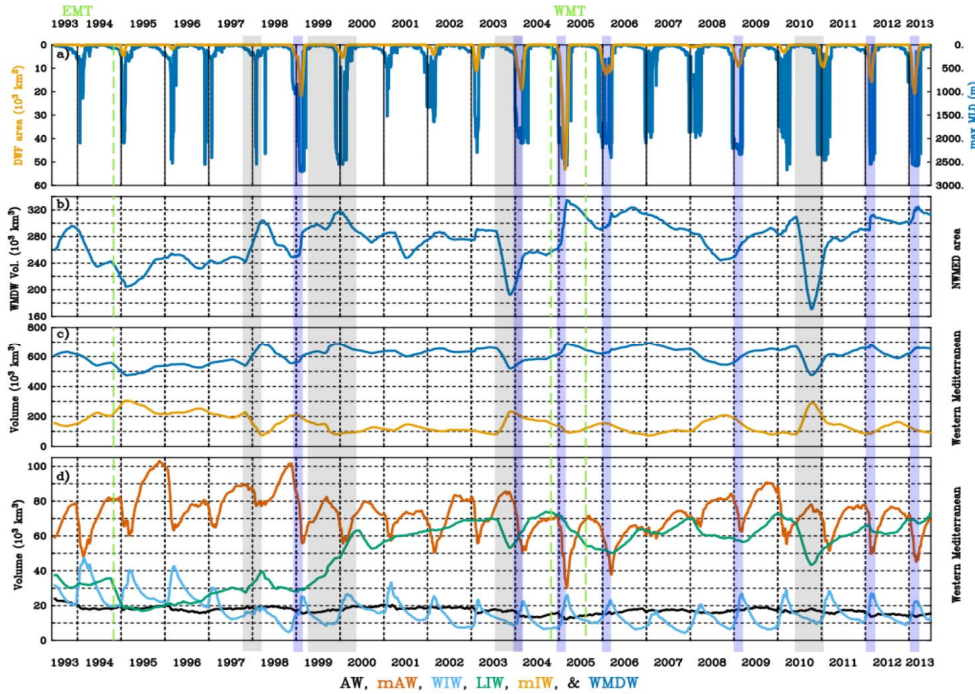
562 **Fig. 5.** Time series of average  $\sigma_{\theta}$  ( $\text{kg m}^{-3}$ , brown lines),  $\theta$  ( $^{\circ}\text{C}$ , blue lines) and  $S$  (green lines)  
 566 characteristics for the Atlantic Water (a), modified Atlantic Water (b), Western Intermediate  
 568 Water (c), Levantine Intermediate Water (e), mixed Intermediate Water (e) and Western  
 569 Mediterranean Deep Water (f).

571 In contrast, the characteristics and volumes of LIWs, mIWs and WMDWs do not vary  
 572 seasonally, but rather show two different dynamics before and after the 1998-2000 period. The  
 573 early years of the simulations show ambiguous thermohaline variations for LIWs, mainly a  
 574 period of slow temperature increase ( $+0.15^{\circ}\text{C}$  in 1993-1995), followed by an increase of both  
 575 temperature and salinity peaking in late 1997, and alternating increases and decreases until the

571 end of 1999. At the same time, the LIW volume starts to slowly increase after 1995, more  
572 suddenly in 1999-2000 and again slowly until 2003 (Fig. 6d). It is constantly high later (about  
573 twice the initial volume of  $30 \times 10^3 \text{ km}^3$ ) but with still some interannual variations ( $\pm 20 \times 10^3$   
574  $\text{km}^3$ ). The thermohaline characteristics and volumes of mIW and WMDW are more stable during  
575 the first four years, but clearly evolve during 1998-2000 toward a higher salinity that remains for  
576 the rest of the reanalysis (+0.04 and +0.02, respectively) and an increased variability. Recalling  
577 that the reanalysis was initiated with results from a twin free run, a longer spin-up than the nine  
578 months initially considered (see section 2.1) could probably explain the questionable variability  
579 observed in the very early years of the reanalysis (1993-1994). The salinization of the middle and  
580 deep layers during 2000 was already noted by [Hamon et al. \(2016\)](#) in a previous version of the  
581 reanalysis (MEDRYS1V1). They attributed it to a biased volume correction term of the SLA  
582 model equivalent. This misfit tends to compensate for the SLA error by densifying the water  
583 columns. As the assimilation system is more constrained on temperature (due to better data  
584 coverage) than on salinity, this adjustment has a stronger effect on salinity, especially at depth  
585 due to the very low number of data assimilated below 600 meters depth before 2005. That being  
586 said, the increase in LIW volume in 1999-2000 does not coincide with the gradual salinization of  
587 LIW that starts earlier and drops off sharply in 1998. Rather, it coincides with an increase of the  
588 LIW flux through the Sardinia Channel (not shown), beginning in late 1998 and peaking (0.35  
589 Sv) in late 1999 -early 2000. This increased LIW flux mainly comes from a slight increase of  
590 salinity (+0.04) of the LIW incoming from the Tyrrhenian, while velocities of the intermediate  
591 layers (200-600m) only show a very slight acceleration ( $+0.01 \text{ cm s}^{-1}$ ). This suggests that the  
592 accumulation of salt and LIW in the Algero-Provençal basin may also be related to the EMT that  
593 slowly propagated higher salt content toward the western Mediterranean from 1997 to 2004  
594 ([Schneider et al., 2014](#); [Amitai et al., 2021](#)). However, this statement must be qualified because  
595 the transport of LIW in the Channel of Sicily does not increase as much as in the Channel of  
596 Sardinia and remains almost constant (not shown). Both processes (i.e., a biased SLA adjustment  
597 or the westward EMT propagation) may have occurred simultaneously but would be difficult to  
598 distinguish since the biased SLA adjustment also affects the Eastern Mediterranean (see [Hamon](#)  
599 [et al., 2016](#), [Beuvier et al., 2016](#)).

600 After 2000, WMDW and mIW show more stabilized behaviors with a variability that is mostly  
601 driven by the interannual variability of DWF, as evidenced by the conversion of mIW to  
602 WMDW (1999, 2005-2006, 2012-2013) and, conversely, a slow decrease (increase) in WMDW  
603 (mIW) volume during periods without DWF (2001-2002, 2007-2008). The effect of DWF is less  
604 pronounced on LIW volume, probably because the algorithm tends to retain the memory of the  
605 LIW salinity anomaly within the newly formed WMDW (see Fig. 3 for example). The WMDW  
606 volume is estimated to be about  $600 \pm 100 \times 10^3 \text{ km}^3$  for the entire area (0 to  $10^\circ\text{E}$ ) and  $270 \pm 30$   
607  $10^3 \text{ km}^3$  when calculated for the same NWMed area as in [Somot et al. \(2018\)](#) (see Fig. 1). This  
608 baseline of WMDW volume is a little higher than in [Rixen et al. \(2005\)](#) and [Somot et al. \(2018\)](#)  
609 (mean of  $185 \times 10^3 \text{ km}^3$  over 1980-2002), mainly due to the algorithm that uses a density  
610 fraction, rather than a fixed density threshold, but the increases in deep water volume during  
611 DWF events ranging about  $50\text{-}180 \times 10^3 \text{ km}^3$  are in good agreement with [Somot et al. \(2018\)](#),  
612 [Beuvier et al. \(2012\)](#), [Waldmann et al. \(2016\)](#) and [Testor et al. \(2018\)](#).

613



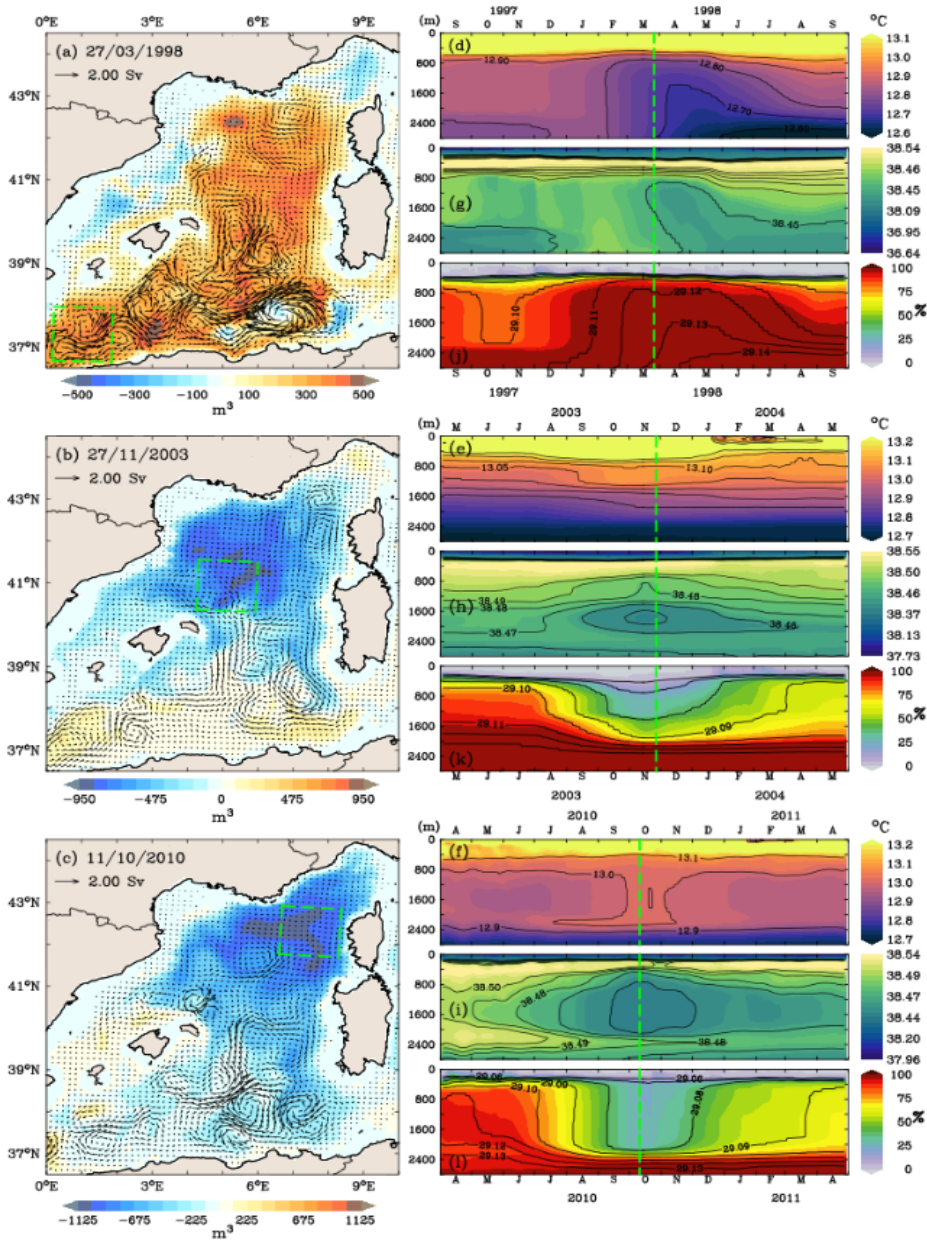
614

615 **Fig. 6.** Time series of the MLD maximum and extent of the DWF area over the NWMED (a) as  
 616 [Somot et al. \(2018\)](#) (see Fig. 1) and volumes of WMDW in the NWMED area (b) and of all the  
 617 water masses over the whole studied area (c, d, see bottom of the figure for the water masses  
 618 color codes). The computations excludes the Alboran and Tyrrhenian Seas. Vertical gray  
 619 color rectangles locate the 1999 LIW accumulation, the 1998 dubious WMDW production event and  
 620 the 2003 and 2010 events of WMDW destruction. Vertical blue rectangles locate the DWF  
 621 periods. EMT and WMT denote Eastern Mediterranean Transient and Western Mediterranean  
 622 Transition.

623 Conversely, some years make exceptions to this behavior, especially 2003 and 2010 showing  
 624 high losses of the LIW (-25% and -40%) and WMDW (-20% and -25%) volumes mirrored by  
 625 gains in mIW volume (about +150% and +250%). Likewise, the year 1998 inversely shows an  
 626 increase (decrease) of the WMDW (mIW) volumes (+27%, -63%) while it is widely recognized  
 627 that 1998 is not a DWF year (e.g. [Somot et al., 2018](#)). These dubious events of WMDW  
 628 production (1998) and mixing or destruction (2003 and 2010) are detailed in Fig. 7. For 1998,  
 629 the WMDW volume anomaly (by reference to the climatological one) suggests that the problem  
 630 originates from the most southwestern area (likely in the Alboran Sea) and propagates  
 631 northeastward on a large part of the basin (Fig. 7a). The associated transport anomalies show a  
 632 considerably strengthened circulation (+2Sv) establishing a large anticyclonic gyre over the  
 633 eastern Algerian basin, which is in contradiction with the well-known cyclonic gyre prevailing in  
 634 this area (e.g., [Send & Testor, 2017](#)). Spatially averaged  $\theta$ -S time series, over the southwestern  
 635 area where the anomaly emerges, show that the WMDW volume anomaly mainly originates  
 636 from a sudden increase of salinity (+0.02) near the bottom in December 1997 (Fig. 7dg) that

637 reaches 1000 m in some months. It is followed by a cooling (-0.15 to -0.27 °C) of similar vertical  
638 extent. These thermohaline changes cause a drastic increase in density over a wide depth range  
639 with the 29.12 kg m<sup>-3</sup> isopycnal reaching 600 m from mid-February to June 1998 (Fig. 7j), this  
640 being too shallow to be realistic in this region. Consequently, the algorithm diagnoses higher  
641 WMDW fractions, leading to dubious increased volumes. The years 2003 and 2010 are inverted  
642 situations with the WMDW volume anomalies showing WMDW destructions located over the  
643 whole Provençal basin (Fig. 7bc). The WMDW transport anomalies are not marked over the  
644 volume anomaly area, likely due to lowered WMDW fractions, but reach ca 1 Sv in numerous  
645 eddy-like structures over a large part of the Algerian basin. These anomalies are due to two  
646 similar events of desalination in the 600-2200 m range lasting several months. The drop in  
647 salinity reached -0.02 in the core (1800 m) of the anomaly in 2003 and -0.03 between 800 and  
648 2000 m in 2010. There is no temperature changes in 2003, but an increase in 2010 that reached  
649 +0.08°C, strengthening the drop in potential density. In both cases, the isopycnals of 29.10 kg m<sup>-3</sup>  
650 fall from 600 to 2000 m (Fig. 7kl), leading the algorithm to diagnose much lower WMDW  
651 fractions (less than 30%) and consequently lower volumes over a large part of the water column.

652 In all of these three cases, there is no physical process that can be invoked to explain such  
653 changes in the salinity and heat contents of deep and intermediate waters over such large areas.  
654 Those are more likely due to biases in the assimilation processes, either through subregional  
655 SLA adjustments or local vertical profiles adjustments, that can propagate over large areas. It is  
656 not in the scope of this study to clearly identify these biases or malfunctioning of the assimilation  
657 processes, but we note that the 1998 event just follow a short period of intensive CTD operations  
658 in the Alboran Sea during the ALMOFRONT-2 campaign (Prieur et al., 2003) while the  
659 availability of CTD profiles in the Mediterranean was generally low before the Argo era (i.e.,  
660 before 2005) and limited to the 0-1000m range (Hamon et al. 2016). The sudden arrival of a  
661 higher level of information at depth in the assimilation system may have over-constrained the  
662 model. Likewise, the 2003 event just follows the 2003 heat wave that has been shown to  
663 markedly impact the SST over the northwestern Mediterranean and the circulation in the Central  
664 Mediterranean (Olita et al., 2007; García-Herrera et al., 2010). It is not unlikely that the model  
665 and/or the assimilation system may have poorly or differently handled the steric effect of this  
666 exceptional heat wave, leading to a destabilization of the assimilation system for the SLA. Note  
667 that WMDW volume calculations using a fixed threshold (such as 29.10 or 29.12 kg m<sup>-3</sup>, Somot  
668 et al., 2018) yielded much more unrealistic estimates during these anomalous events, with  
669 stronger and more sudden variations (a few days, not shown). This indicates that the problem  
670 does not come from the water mass detection algorithm and rather supports the hypothesis of  
671 accidental biases in the assimilation system.



673 **Fig. 7.** Anomalies of the WMDW volumes (by reference to the climatology of Fig. 4f) at the  
674 dates of maximum of the anomalous events of 1998 (a), 2003 (b) and 2010 (c), and  
675 corresponding year-long centered time series of spatially averaged temperature (d, e, f), salinity  
676 (g, h, i) and WMDW ratio (j, k, l) in the most impacted areas. The black arrows on the left panels  
677 show the WMDW transport anomalies. The green squares show the spatial domains used for  
678 averaging time series. The vertical green lines on right panels indicate the same day as on the left  
679 panels. Isopycnals ( $\text{kg m}^{-3}$ ) are shown on the WMDW fractions' time series.

680 Beyond that, the reanalysis seems to resist these artifacts, which do not last more than a few  
681 months in terms of water mass volume (Fig. 6) and characteristics (Fig. 5). The impact in terms  
682 of deep water transport is more questionable, especially for the 1998 event for which the increase  
683 in WMDW transport over the Algerian basin and the inverted barotropic gyre lasted a few more  
684 than two years. We therefore recalculated the long-term mean volumes and transports for each  
685 water mass without the years 1998-1999, 2003, and 2010, as shown in Fig. 8. There are no  
686 significant differences in the volumes and transports of AW, mAW and WIW between Fig. 4 and  
687 Fig. 8 showing that the dubious events have had no effect on surface water masses. The new  
688 estimates for LIW, mIW and WMDW better highlight a deep cyclonic gyre in the eastern  
689 Algerian basin that is much more consistent with the literature (Testor et al., 2005b; Send &  
690 Testor, 2017). This mean cyclonic gyre was hidden by the strong anticyclonic gyre generated by  
691 the suspicious 1998 WMDW event, maintained until early 2000. The mIW and LIW also now  
692 exhibit this deep cyclonic circulation (Mallil et al., 2021), leading to cumulative transports of  
693 deep and intermediate water mass of about  $2.5 \pm 0.5\text{Sv}$ , only slightly lower than those reported  
694 by Send & Testor (2017) ( $4.0 \pm 1.0\text{Sv}$ ). For the six water masses, the largest volume differences  
695 from the first guess appear primarily in the western Algerian basin, consistent with the removal  
696 of the 1998 WMDW event, but do not exceed 10%.

### 697 3.3. Possible Connections of Deep and Surface Dynamics

698 The corrected climatology of water mass circulations (Fig. 4) highlights a deep gyre in the  
699 eastern Algerian basin in controlling the dynamics of deep and intermediate water masses. It has  
700 been suggested previously that this deep gyre may also control the surface path of AEs (Isern-  
701 Fontanet et al., 2006; Escudier et al., 2016; Pessini et al., 2018; Mallil et al., 2021). Although  
702 clearly an artifact, the 1998 WMDW production event in the Alboran Sea suggests that the deep  
703 gyre of the eastern Algerian basin may be highly sensitive to the arrival of newly formed deep  
704 water. In addition, Barral et al. (2021) showed that the DWF over the northern sub-basin can  
705 shift the northern boundary of the AEs, i.e. the Balearic-Sardinian frontal zone, one degree  
706 southward. They hypothesized that this would be due to a weakening in the formation and  
707 northward propagations of AEs during DWF years. To reexamine this hypothesis, we  
708 recomputed the mean water mass volumes and transports by separating the years with (2004-  
709 2006, 2009, 2011-2012, 6 years mean) and without DWF (1993-1997, 2000-2002, 2007-2008, 10  
710 years mean) based on the maximum MLD and DWF area (Fig. 6a).



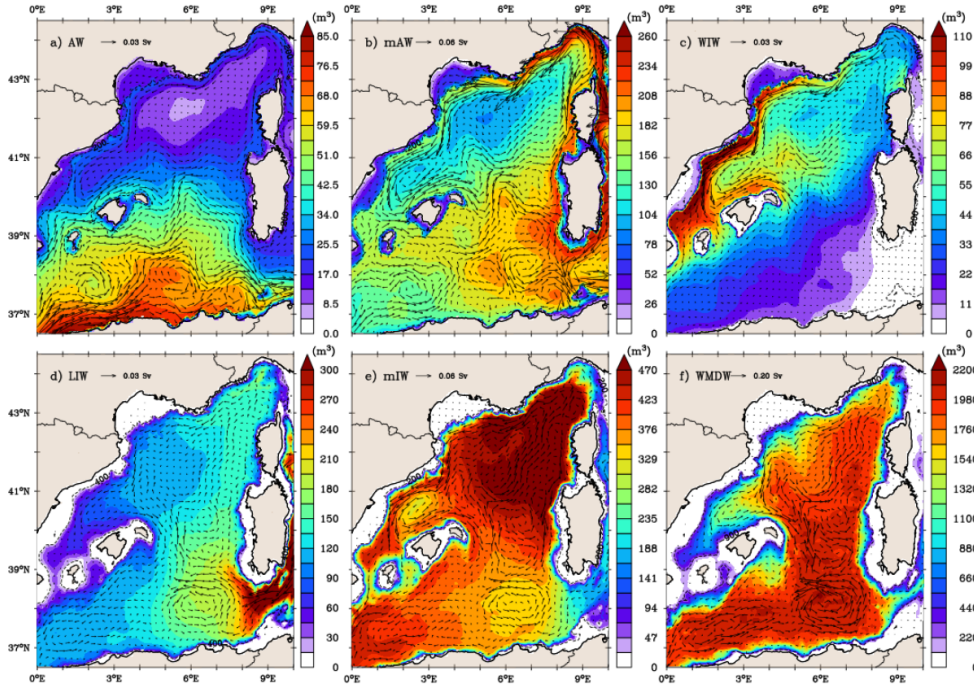


**Fig. 8.** Same as Fig. 4, without the years 1998-1999, 2003 and 2010.

711 For each water mass, the difference in mean volumes and transports between the two regimes are  
 712 presented in Fig. 9. Years with DWF correctly show larger volumes of WMDW in the  
 713 northwestern part of the basin, mainly in the known DWF area around 42°N-5°E, as well as  
 714 increased transport of WMDW from the DWF area to northern Menorca and southward. The  
 715 volume differences over the central Liguro-Provençal area for the mAW, WIW and mIW  
 716 illustrate the conversion of surface and intermediate waters to WMDW when DWF occurs. The  
 717 LIW volume is higher over the entire basin during DWF years in contradiction with the usual  
 718 finding of its destruction during DWF events. This is partly due to the algorithm that retains  
 719 memory of the LIW in deep layers after DWF events (see Sec. 3.1 and Fig. 3), but may also  
 720 reflect the 1999 increase in LIW volume (Section 3.2), as all of the used DWF years occur after  
 721 2004. Furthermore, the differences in transport estimates show an acceleration of the along-slope  
 722 cyclonic circulation over the Liguro-Provençal area for all surface and intermediate water  
 723 masses. This acceleration of the regional cyclonic circulation has been suggested for a long time,  
 724 based on heat and water budget (e.g., [Bethoux et al., 1982](#); [Astraldi & Gasparini, 1994](#)) or  
 725 dynamical considerations (e.g., [Crépon & Boukthir, 1987](#); [Madec et al., 1991](#)) and clearly  
 726 evidenced in dedicated modeling study (e.g., [Hermann et al., 2008](#)) but, to our knowledge, never  
 727 on such climatological mean. Except for a thin area on the west coast of Corsica which will be  
 728 discussed later, the water mass volumes over the northern along-slope circulation are not  
 729 significantly affected, showing that the response is almost kinematic. Conversely, there are

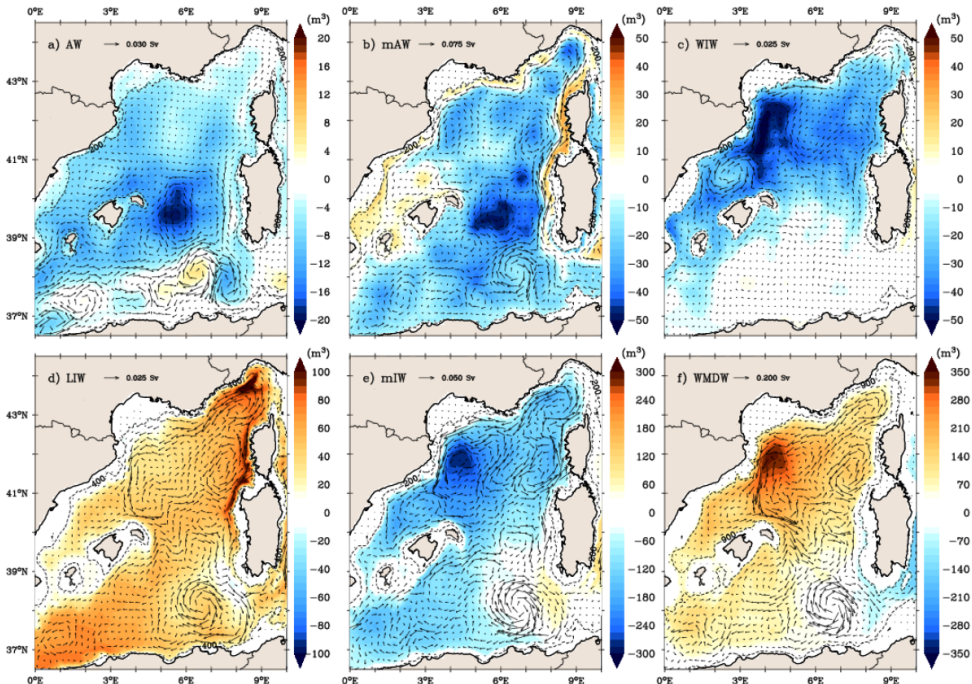
730 significant changes in the AW volumes around and east of the Balearic Sea, showing that the  
731 shape of the northern (southern) extension of the AW (mAW) reservoir is modified toward less  
732 AW north of 39°N. This is consistent with our previous study that shows a DWF-induced  
733 meridional shift of the haline frontal zone that prevails between Menorca and Sardinia (Barral et  
734 al. 2021). This regime shift also largely affects the amount of mAW at the West of Sardinia and  
735 above the Algerian gyre, suggesting that less mAW may be produced by mixing in the AEs or to  
736 a lesser extent and activity of the AEs following a DWF event.

737 The difference in transports estimates between the two regimes also shows a marked inversion of  
738 the deep circulation in the area of the eastern deep Algerian gyre when DWF occurs, comforting  
739 the hypothesis of a disruption, or at least, a marked weakening of the barotropic gyre in response  
740 to the increased southward flow of the WMDW. Except WIW which is not detectable in this  
741 region, all the surface (AW, mAW) and intermediate (LIW, mIW) water masses show the same  
742 tendency. For LIW and mIW, this is likely due to the algorithm that maintains a link between the  
743 intermediate water masses and the WMDW through the use of salinity and potential density  
744 fractions, but it is also coherent with Send and Testor (2017). The alignment between the  
745 circulations of surface (AW, mAW) and deep water masses over the eastern deep Algerian gyre  
746 is less intuitive, but not so surprising if this long term mean is seen as retaining the long-term  
747 average of the paths of the AEs as guided by the deep barotropic gyre (Isern-Fontanet et al.,  
748 2006; Escudier et al., 2016; Pessini et al., 2018; Mallil et al., 2021). The weakening of the deep  
749 eastern Algerian gyre would induce a lesser northern extent of the AEs, as suggested above  
750 regarding the differences in AW and mAW volumes, hence a weakened signature of their paths  
751 on the surface circulation.

752 Surprisingly, it is not 2005, the most convective year in the time series (Fig. 6a, Schroeder et al.  
753 2008a; Somot et al., 2018), that have the largest effect on the annual circulations of surface and  
754 intermediate water masses, but the year 2009 with an overflow of WMDW towards the  
755 Tyrrhenian that induced a strong return current of mAWs at the surface. This 2009 event is  
756 clearly visible on the upper panel of Fig. 10 which shows the water mass fluxes through the  
757 Sardinia Channel. The transports of WMDW and mAW differ from the rest of the time series,  
758 from mid-2008 to the end of 2009, both in intensity (larger than 1Sv) and sign, and are almost  
759 perfectly opposite. This overflow of the WMDW onto the sill in 2009 has been previously  
760 documented (Schroeder et al., 2016) and is attributed to the deposition on the seafloor in 2005 of  
761 the newly formed WMDWs, followed by several moderate DWF events in 2006, 2008 and in  
762 2009. Each of these DWF events results in successive WMDW deposition, year after year, with  
763 the top of accumulated WMDW reaching 1900 m in 2009, the depth of Sardinia Channel sill  
764 (e.g. Schroeder et al., 2016; Li and Tanhua, 2020; Ben Ismail et al., 2021). The two transport  
765 anomalies peak late-June 2009, 4 months after the 2009 DWF events, a time scale for WMDW  
766 propagation that is consistent with Schroeder et al (2008a) and Beuvier et al (2012).

767

Formatted: Font: (Default) Times New Roman,  
Pattern: Clear



768

769 **Fig. 9.** Differences of water mass volumes and transports between the average of 10 years  
 770 without DWF and the average of 6 years with DWF (i.e., DWF minus no DWF) for Atlantic  
 771 Water (a), modified Atlantic Water (b), Western Intermediate Water (c), Levantine Intermediate  
 772 Water (e), mixed Intermediate Water (e) and Western Mediterranean Deep Water (f). A scale  
 773 arrow for transport values is shown on each panel.

774 The time series of AW transport shows that it is not modified in the Channel of Sardinia in  
 775 comparison with the previous years (still stronger in winter than summer), but its spatial  
 776 distribution is more strongly affected (Fig. 10a) leading to a significant redistribution of the  
 777 amount of AW over the whole basin. This redistribution shows a smaller volume of AW over the  
 778 Balearic Islands contrasting with an accumulation in the eastern Algerian sub-basin in several  
 779 AEs. In addition, part of the AW is driven by the northward flow of mAW from the center of the  
 780 Algerian basin into the WCC. This unusual AW spatial distribution is consistent with [Barral et](#)  
 781 [al. \(2021\)](#) who reported an anomalous northward extension of the AW-mAW haline frontal zone  
 782 in 2009, while DWF years are generally characterized by a southward migration of the haline  
 783 front. The lower amount of AW around the Balearic Archipelago is clearly due to the increased  
 784 influx of mAW in the Balearic Sea and the WIW anticyclonic structures, preventing the usual  
 785 northward summer inflow of AW through the Balearic channels (e.g., [Mason & Pascual, 2013](#);  
 786 [Vargas-Yanez et al., 2020](#)).

787 The transports of LIW and mIW through the Sardinia Channel are also modified after this  
 788 exceptional event, but at a lower level and with a 6-month delay. Again, the impact is more  
 789 pronounced on their regional circulations throughout the basin. The positive anomaly of LIW  
 790 volume over the entire Algero-Provençal basin is coherent with Fig. 9d as 2009 is a DWF year..

791 The greater amount in the Ligurian is likely due to the northward accumulation and entrainment  
 792 by the mAW flow, while the negative LIW volume anomaly in the Sardinia Channel may reflect  
 793 the thinning of the LIW layer due to the larger inflow of mAW and the larger outflow of  
 794 WMDW. The amount of mIW decreases throughout the basin, first because of the winter DWF  
 795 in the Provençal basin (as shown in Fig. 9e), and second because mIW is trapped between a  
 796 shallower WMDW upper boundary and a deeper AW/mAW lower boundary, especially over the  
 797 shelf slope of western Sardinia and Corsica (Fig. 3hkl).

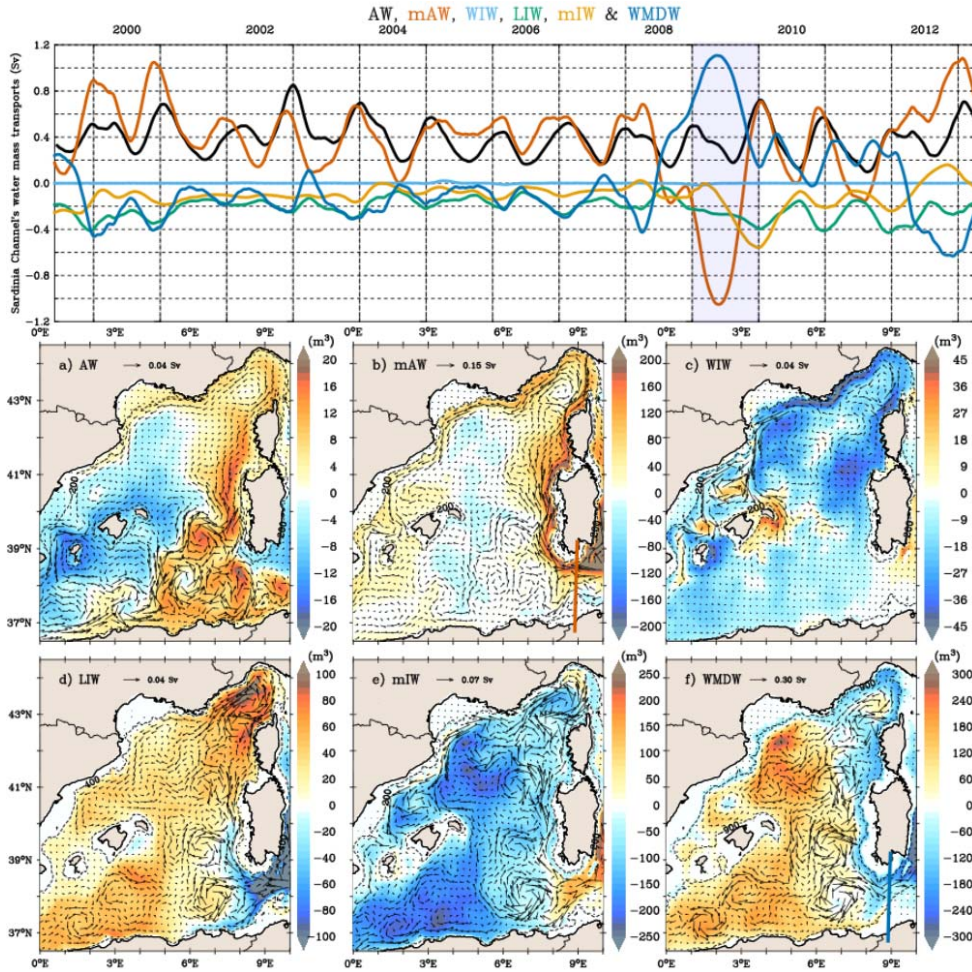


**Fig. 10.** Time series of water mass transport (Sv, positive eastward) through the Sardinian Channel (upper panel, water mass color codes shown at the top and volume and water mass transport anomalies in 2009 compared with the climatology of Fig. 8 (lower panels) for Atlantic waters (a), modified Atlantic waters (b), western intermediate waters (c), Levantine intermediate waters (e), mixed intermediate waters (e) and deep western Mediterranean waters (f). The section of the Strait of Sardinia is shown in panels b and f. Transport values in the upper panel are smoothed using a seasonal triangular filter.

798

#### 799 4. Discussion and Conclusion

800 The main objective of this study was to extract from a 20-year reanalysis of the Western  
 801 Mediterranean a coherent climatological picture of the water mass dynamics, focusing on the  
 802 Algero-Provençal basin. To do this, we built a  $\theta$ -S based algorithm that discriminates the main  
 803 water masses in order to estimate the corresponding volumes and transports. Prior to the actual  
 804 analysis, the calculated water mass mixing fractions were also used to estimate the mean  
 805 thermohaline characteristics and depth range of each water mass. This allowed us to validate the  
 806 behavior of the algorithm, i.e., to ensure that it could indeed report the correct water mass at the  
 807 correct depth. Averaged over the 20 years of the reanalysis, the results give consistent  
 808 distributions of the volumes and transports of the different water masses. The AW is mainly  
 809 located in the AC and spread by the AEs over a large part of the Algerian basin. The mAW is  
 810 produced in the area of AEs influence and flows cyclonically over most of the continental slopes  
 811 of the basin. The WIW is produced in the Liguro-Provençal basin and the Gulf of Lion and  
 812 accumulated in the Balearic Sea. The LIW is flowing and diluting towards the northwest, mainly  
 813 by the SEs. The WMDW is produced by regular and realistic deep convection events in the  
 814 Provençal area and flows southwards to accumulate in the deeper Algerian basin. The analysis of  
 815 the time series of temperature, salinity and volumes brought several other positive elements, such  
 816 as the coherent seasonally driven variability of AW, mAW and WIW, and the realistic inter-  
 817 annual variability of WMDW production, particularly in 2005 which is known to be the major  
 818 DWF event of the last three decades, given its impact on the intermediate and deep thermohaline  
 819 characteristics (Schroeder et al., 2008ab).

820 This sudden exchange of mAW and WMDW between the Tyrrhenian and the Algero-Provençal  
 821 basin leads to important changes in the regional distribution and circulation of surface and  
 822 intermediate water masses over the whole western basin. The marked mAW influx from the  
 823 Tyrrhenian induces a continuous flow along western Sardinia and Corsica that feeds the WCC  
 824 and the NC as far as the Balearic Sea (Fig. 10b). The concomitant increase in mAW volume is  
 825 likely responsible for the difference in mAW between years with and without DWF previously  
 826 observed in Fig. 9b along western Sardinia and western Corsica, as well as the maximum peak in  
 827 mAW volume over the entire basin in 2009 in Fig. 6d. Likewise, this arrival of warmer mAW  
 828 from the Channel of Sardinia through the WCC leads to a negative anomaly in the WIW volume  
 829 along the Liguro-Provençal continental slopes (Fig. 10c) whereas the lack in WIW around 42°N-  
 830 5°E is consequent to the consumption of WIW by the 2009 DWF. The volume anomaly of WIW  
 831 in the Balearic Sea shows increased escapes in the Ibiza Channel and northeast of Menorca,  
 832 somewhat pushed by the mAW influx, but also the persistence of two distinct anticyclonic  
 833 structures accumulating WIW in the central area and north of Ibiza. This latter has been reported

834 in [Mason & Pascual \(2013\)](#) as an anomalous SLA pattern in 2009, standing all year long but  
835 strengthened in Autumn.

836 Nevertheless, the times series also reveal spurious anomalies in the intermediate and deeper  
837 layers as mIW-WMDW coupled nonphysical variability in 1998-1999, 2003 and 2010 that have  
838 been assigned to assimilation biases. Those are due to subtle variations of salinity (0.02-0.04)  
839 slightly lowering (for the 2003 and 2010 cases) or hardly increasing (for the 1998-1999 case)  
840 potential density on a large part of the intermediate and deep waters. From this point, the  
841 somewhat fuzzy definition of the mIW may appear as the main shortcoming of our approach and  
842 should be discussed first. The mIW aggregates several water masses of diverse origins, such as  
843 TDW (which itself has diverse origins, e.g., [Fuda et al., 2002](#); [Buffet et al., 2017](#); [Li & Tanhua,](#)  
844 [2020](#); [Iacono et al., 2021](#)) and any waters possibly formed during intermediate or moderate  
845 convective events, and that do not fall into the typical WMDW category (such as the WDW in  
846 [Bosse et al., 2016](#)). The different intermediate water masses included in the mIW may have  
847 similar thermohaline characteristics and are distributed mainly along a LIW-WMDW mixing  
848 line. As such, they do not generate an inflection point on the  $\theta$ -S diagram that could help to  
849 clearly discriminate them. Similarly, the algorithm does not distinguish Tyrrhenian Intermediate  
850 Water (TIW), a slightly warmer equivalent of the WIW formed in winter due to the Mistral  
851 channeled through the Strait of Bonifacio ([Napolitano et al., 2019](#); [Iacono et al., 2021](#)). The TIW  
852 flows northward to the Corsican Channel and dilutes in the NC with average characteristics  
853 ( $\theta \sim 14^\circ\text{C}$ ,  $S \sim 38.3$  and  $\sigma_\theta \sim 28.8 \text{ kg m}^{-3}$  in the reanalysis) similar to the mAW. The ideal way to  
854 properly sort TIW from the WIW-mAW set, and TDW from the mIW set, would be Lagrangian  
855 tracking of these water types along their trajectories from their original locations. This method  
856 has a development and computational cost that was quite prohibitive given the encouraging  
857 results we obtained with very early versions of the  $\theta$ -S based algorithm (see [Barral et al. 2020](#)).  
858 Indeed, the presently defined mIW pool may be related to the finding of [Millot \(2013\)](#) as  
859 representative of all intermediate waters produced in areas of convection in the eastern basin, but  
860 extended here to the western basin as well. As so, it has an oceanographic sense, even if an  
861 oversimplified one, and it is not at the origin of the problem. Instead, its use helped to identify  
862 the three WMDW anomalous events.

863 Second, the regime shift suggested by the marked increase of the estimated LIW volume (briefly  
864 discussed in section 3.2) call for a discussion on the fact that the current algorithm does not take  
865 into account the warming and salinization trends observed throughout the Mediterranean in  
866 recent decades (e.g., [Schroeder et al., 2017](#); [Iona et al., 2018](#); [Skliris et al., 2018](#); [Vargas-Yanez](#)  
867 [et al., 2021](#); [Fedele et al., 2022](#)). Warming would not significantly affect water mass sorting  
868 when based on salinity ratio (i.e., for AW, mAW, and LIW), but would eventually lead WIW to  
869 be less marked and even disappearing, at least relative to their current definition. [Juza et al.](#)  
870 [\(2019\)](#) and [Vargas-Yanez et al. \(2021\)](#) showed a warming trend in WIW of 0.14-0.5°C over the  
871 last decade, but our results do not show a significant decrease in the amount of WIW over the  
872 1993-2013 period. This can be explained by recalling that the current algorithm progressively  
873 marks WIW for a temperature below 13.5°C, whereas the usual temperature threshold used to  
874 identify it is 13°C. Preliminary tests using lower thresholds led to large underestimations of  
875 WIW volumes. The WIW temperature threshold was then set to keep the WIW volume estimates  
876 within the range of previous estimates and it appears, therefore, to implicitly parameterize the  
877 recent warming of the WIW. The most recent estimates of salinity trends in the Western  
878 Mediterranean range from 0.002 to 0.007  $\text{yr}^{-1}$  depending on the area and period covered ([Iona et](#)  
879 [al., 2018](#); [Skliris et al., 2018](#); [Vargas-Yanez et al., 2021](#); [Fedele et al., 2022](#)). Taking the most

880 extreme estimates, salinity changes over a 20-year period remain small (0.04-0.14) relative to the  
881 salinity ranges used by the algorithm to differentiate AW from mAW (2.35) and mAW from  
882 LIW (0.55). Furthermore, this trend appears to be more pronounced for AW than LIW (e.g.,  
883 [Vargas-Yanes, 2021](#); [Fedele et al., 2022](#)) so we do not expect serious bias in their fraction  
884 estimates. The problem is more questionable for the density-based water column partitioning,  
885 mainly for mIW-WMDW sorting which is very sensitive to small changes in potential density, as  
886 seen with the three anomalous events detected with the algorithm. Nevertheless, due to the  
887 nonlinear and antagonistic impact of salinity versus temperature changes on the sea state  
888 equation, the potential density trends observed for LIW or WMDW in the Western  
889 Mediterranean are small or insignificant (e.g., [Vargas-Yanez et al., 2021](#)) compared to the  
890 potential density values used in the algorithm to partition the water column. Therefore, we  
891 conclude that these warming and salinity trends would not have biased the estimated water mass  
892 fractions, and thus the subsequent volume and transport estimates. Nevertheless, it is clear that  
893 careful a priori consideration will be required for application on a longer time scale than the  
894 present 20 years analysis.

895 Validation or evaluation of a reanalysis is most often based on global statistics for heat and salt  
896 content, model misfit or assimilation increment, etc. (e.g., [Hamon et al., 2016](#); [Aznar et al.,  
897 2016](#)). The approach we used goes further in this necessary assessment exercise as it allows us to  
898 identify at least three unrealistic events over the deep and intermediate layers that would be  
899 undetectable from global statistics given the small value of the salinity and temperature biases  
900 involved (fewer than 0.1, and than 0.3 °C). In fact, similar biases are likely to occur throughout  
901 the water column, but their impact would be much lower in the surface layers given the higher  
902 range of salinity and temperature variability between AW, mAW and WIW. Indeed, the removal  
903 of the three anomalous episodes shows no impact on surface volumes and circulations. This  
904 highlights a general weakness of contemporary reanalyses, which most often start in 1993 to  
905 benefit from the availability of altimetry data, but thus cover periods of very heterogeneous  
906 availability of in situ data. In the Mediterranean, the start of the ARGO era between 2000 and  
907 2005 has led to a fivefold increase in available in situ profiles, but with still insufficient coverage  
908 of deep layers, especially for salinity (e.g., [Hamon et al., 2016](#)). Because deep salinity is the least  
909 constrained variable in assimilation systems, it is the most likely to suffer from assimilation bias.  
910 Nevertheless, we have shown that bypassing the biased periods allowed us to improve the  
911 average circulation scheme of the intermediate and deep water masses, mainly by retrieving the  
912 well known eastern Algerian barotropic Gyre (see Fig. 8def). This shows that the reanalysis is  
913 robust to accidental assimilation biases and we can expect deep-sea dynamics to be better  
914 constrained as more and more in situ deep-sea data become available for assimilation.

915 Beyond the assessment exercise, this study suggests new findings regarding the impact of the  
916 WMDW dynamics on surface and intermediate waters. The first is a possible breakdown of the  
917 eastern Algerian barotropic Gyre in response to the arrival of new WMDW in the southern part  
918 of the basin following significant DWF events occurring in the northern part. This disturbance of  
919 the Algerian Gyre has not been documented before from in situ data, but can be seen in [Beuquier  
920 et al. \(2012\)](#) who describes the southward propagation of WMDW cyclonic eddies after the  
921 strong DWF event of 2005 leading to a similar destabilization of the gyre in a model. Note that  
922 this deep gyre is not a true permanent feature in the reanalysis, but the average effect of the paths  
923 of several smaller (50-100 km) anticyclonic eddies. The velocities (and hence transports) in these  
924 eddies are about half the velocities of the southward spreading cyclonic eddies of the newly  
925 formed WMDW (about 5 cm s<sup>-1</sup> vs 10 cm s<sup>-1</sup>, [Testor et al. 2005b](#); [Beuquier et al., 2012](#)). The

926 resulting eddy-eddy interactions are complex and chaotic (e.g., Waldman et al., 2018; Testor et  
927 al., 2018), so the disturbance of the deep gyre may simply reflect the mean of a more turbulent  
928 deep circulation. Of the sixteen years used to compute the two average regimes (i.e., after  
929 elimination of the four biased ones), six are DWF years while ten do not and DWF years occur  
930 more often at the end of the reanalysis, so that the two climatological regimes do not have the  
931 same statistical robustness. Nevertheless, the differences between the two regimes (DWF or no  
932 DWF) are coherent with the known acceleration of the northern cyclonic circulation of the  
933 surface (mAW), subsurface (WIW) and intermediate (LIW and mIW) layers (e.g., Madec et al.,  
934 1991; Herrmann et al., 2008), and with the southern shift of the AW/mAW main frontal zone  
935 suggested in Barral et al. (2021) during DWF years. The last issue concerns the deep water  
936 overflow in the Sardinia Channel following the 2009 DWF event, and its drastic impact on the  
937 circulations of intermediate and surface waters (Fig. 10). This overtopping is documented by  
938 Schroeder et al. (2016) as following the strong deep water renewal of 2005, the WMT, on which  
939 several other episodes accumulated from 2006 to 2010, bringing the upper boundary of deep  
940 water above the sill depth. The reanalysis appears to replicate this complex accumulation  
941 sequence over several years. The subsequent impact of the WMDW overflow on the AW, mAW,  
942 and WIW circulations seems globally coherent (discussed in more detail in Section 3.3), but the  
943 2010 deep assimilation anomaly spoils the end of this sequence. Moreover, we did not find any  
944 independent estimate to validate the across strait eastward (westward) WMDW (mAW)  
945 transports (order 1 Sv) computed during the overflow event. Given the problems detected  
946 regarding the deep water dynamics in this reanalysis, more investigation will be needed to better  
947 corroborate these new findings regarding the impact of the DWF over surface and intermediate  
948 water mass dynamics throughout the Western Mediterranean. The way to do this are in progress  
949 by analyzing the satellite altimetry observations and, with the same algorithm of water mass  
950 sorting and derived proxies (volumes, transports), the twin free run of the MEDRYS1V2  
951 reanalysis and another longer and finer reanalysis of the Mediterranean, precisely the CMEMS-  
952 MedRea reanalysis (1987-2019, 1/24°, Escudier et al., 2021). This should allow us to compare  
953 the impact of the detected assimilation biases, to get more robust climatological estimates and to  
954 enlarge the studied area to the Alboran and Tyrrhenian Seas.

955

#### 956 **Acknowledgements**

957 This work was part of the PhD thesis of Q.-B. Barral funded by the French Ministère de  
958 l'Enseignement Supérieur, de la Recherche et de l'Innovation (MESRI). It is a contribution to the  
959 MISTRALS (Mediterranean INtegrated STudies at Regional And Local Scales) program through  
960 the CLOSCHMED (CLOSure SCHEME of the MEDiterranean gyre) project funded by the  
961 French CNRS/INSU program LEFE-GMMC.

962

#### 963 **Appendix A : The detection algorithm of water masses in the Western Mediterranean.**

964 First step of the algorithm, the partitioning of the water column involves the definitions of  
965 surface and deep layers. To locate the surface layer, two densities bound a linear function  
966 between the mAW ( $\sigma_{mAW}$ ) and the LIW ( $\sigma_{LIW}$ ). Above this  $\sigma_{mAW}$ , the surface flag is set to one  
967 while below  $\sigma_{LIW}$ , it is set to zero as :



$$968 \quad flag_{surf} = \begin{cases} 1, \sigma < \sigma_{mAW} \\ \frac{\sigma_{LIW} - \sigma}{\sigma_{LIW} - \sigma_{mAW}}, \sigma_{mAW} \leq \sigma \leq \sigma_{LIW} \\ 0, \sigma > \sigma_{LIW} \end{cases} \quad (A.1)$$

969 where  $\sigma_{mAW}=28.9643 \text{ kg m}^{-3}$  (computed from  $S_{mAW}=38.45$ ,  $\theta_{mAW}=13.5^\circ\text{C}$ ) and  $\sigma_{LIW}=29.061 \text{ kg}$   
 970  $\text{m}^{-3}$  ( $S_{LIW}=39$ ,  $\theta_{WMDW}=15^\circ\text{C}$ ), standing for the lower bound of the surface layer and the well  
 971 known core of the intermediate layer, respectively.

972 The separation of the deep layer of the water column from the intermediate is carried out in the  
 973 same way, but between the LIW and WMDW :

$$974 \quad flag_{deep} = \begin{cases} 0, \sigma < \sigma_{LIW} \\ \frac{\sigma - \sigma_{LIW}}{\sigma_{WMDW} - \sigma_{LIW}}, \sigma_{inf} \leq \sigma \leq \sigma_{WMDW} \\ 1, \sigma > \sigma_{WMDW} \end{cases} \quad (A.2)$$

975 where  $\sigma_{LIW}$  remains as previously, and  $\sigma_{WMDW} = 29.1075 \text{ kg m}^{-3}$  is computed from  
 976  $S_{WMDW}=38.45$ ,  $\theta_{WMDW}=12.815^\circ\text{C}$ .

977 The second step sorts the freshwater as a water with a salinity which is lower than the AW  
 978 salinity minimum ( $S_{AW}=36$ ) :

$$979 \quad flag_{fresh} = \begin{cases} \frac{S_{AW} - S}{S_{AW}}, S \leq S_{AW} \\ 0, S > S_{AW} \end{cases} \quad (A.3)$$

980 The flagging of AW hence uses a salinity ratio built to represent the AW-mAW mixing in the  
 981 surface layer :

$$982 \quad flag_{AW} = \begin{cases} (1 - flag_{fresh}) \cdot flag_{surf}, S < S_{AW} \\ \left( \frac{S_{mAW} - S}{S_{mAW} - S_{AW}} \right) \cdot flag_{surf}, S_{AW} \leq S \leq S_{mAW} \\ 0, S > S_{mAW} \end{cases} \quad (A.4)$$

983 The LIW is defined assuming no salinity is higher than 39 in the western basin and that it dilutes  
 984 along a salinity gradient from 39 to 38.45 (the mAW salinity maximum) :

$$985 \quad flag_{LIW} = \begin{cases} 0, S < S_{mAW} \\ \frac{S - S_{mAW}}{S_{LIW} - S_{mAW}}, S \geq S_{mAW} \end{cases} \quad (A.5)$$

986 The sum of previous water mass fractions defines a temporary flag that allows only the  
 987 remaining ratios to be treated :

$$988 \quad tmp = flag_{fresh} + flag_{AW} + flag_{LIW} \quad (A.6)$$

989 Sorting the mAW and WIW assumes that they are pooled in the remaining surface waters and  
 990 can be discriminated using a temperature ratio :

$$991 \quad flag_{WIW} = flag_{surf} \cdot (1 - tmp) \cdot ratio_{WIW} \quad (A.7a)$$

992

$$993 \quad flag_{mAW} = flag_{surf} \cdot (1 - tmp) \cdot (1 - ratio_{WIW}) \quad (A.7b)$$

994 where :

$$995 \quad \sigma < \sigma_{LIW} \Rightarrow ratio_{WIW} = \begin{cases} 1, \theta < \theta_{WIW} \\ \frac{\theta_{mAW} - \theta}{\theta_{mAW} - \theta_{WIW}}, \theta_{WIW} \leq \theta \leq \theta_{mAW} \\ 0, \theta > \theta_{mAW} \end{cases} \quad (A.8)$$

996 The last well-known water mass to define is WMDW which is simply located with the potential  
997 density ratio of (A.2) in the remaining waters of (A.6) :

$$998 \quad flag_{WMDW} = (1 - tmp) \cdot flag_{deep} \quad (A.9)$$

999 All known water masses being defined, mIW are defined as the rest of all flags :

$$1000 \quad flag_{mIW} = 1 - (flag_{fresh} + flag_{AW} + flag_{mAW} + flag_{WIW} + flag_{LIW} + flag_{WMDW}) \quad (A.10)$$

1001

## 1002 **Appendix B : The characteristics, volumes and transports of the water masses.**

1003 The mean characteristics ( $\theta$ ,  $S$ ,  $\sigma_\theta$  and depth) of each water mass is computed as flag and volume  
1004 weighted means, as for example for the mean potential temperature :

$$1005 \quad \bar{\theta}_i(t) = \frac{\sum_{xyz}(flag_i \cdot \Delta x \Delta y \Delta z \cdot \theta)}{\sum_{xyz}(flag_i \cdot \Delta x \Delta y \Delta z)} \quad (B.1)$$

1006 where “i” is the water mass index (from 1 to 6 : AW, mAW, WIW, LIW, mIW, WMDW) and  
1007 dx, dy and dz are the spatial increments defining the finite volume of one grid mesh. Note that  
1008 the model grid being curvilinear and bottom adjusted for the deepest wet grid meshes (partial  
1009 step discrete mesh), the grid meshes dimensions vary in space. Indexes of spatial increments  
1010 have been omitted for simplification in this and the following equations (except when essential).  
1011 The estimate for the core of a water mass is similarly computed but retaining only the value of  
1012 the maximum fraction inside each vertical profile.

1013 Starting for a simple water column (i.e., at a fixed longitude and latitude location), the water  
1014 mass volume is computed as :

$$1015 \quad V_i(x, y, t) = \int_z flag_i \cdot dV = \sum_z flag_i(x, y, z, t) \cdot \Delta x \Delta y \Delta z \quad (B.2)$$

1016 This first quantity allows us to construct daily maps of the volumes of the different water masses.  
1017 Suming over the whole domain (or a subdomain like for the NWMed area) leads to the total  
1018 volume of each water mass. As the local (x,y,z,t) sum of all the water mass flags is always one, it  
1019 is straightforward to show that the summing over all water masses gives the constant water  
1020 column volume that is only bathymetry dependent, neglecting the dynamic height (SSH) that is  
1021 only about a tens of centimeters over the Western Mediterranean.

1022 Using the same flags based distribution principle, each water mass transport (Sv) over a water  
1023 column is computed as :

$$1024 \quad \vec{M}_i(t) = \iint (flag_i \cdot \vec{U}) ds \approx \vec{i} \sum_k (flag_i \cdot u_\theta \cdot \Delta x_\theta \Delta z_\theta) + \vec{j} \sum_k (flag_i \cdot v_\theta \cdot \Delta y_\theta \Delta z_\theta) \quad (B.3)$$

1025 where “ $u_\theta$ ” and “ $v_\theta$ ” stand for the velocity components interpolated at the scalar (temperature and  
1026 salinity) grid points, according to the used curvilinear and Arakawa C mesh grid. Similarly, the  
1027 across-section transports are computed as :

$$1028 \quad M_i^S(t) = \iint (flag_i \cdot \vec{U} \cdot \hat{n}) ds \approx \sum_{N_S} \sum_k [flag_i \cdot (u_S \cdot \Delta x_u \cdot \Delta z_u + v_S \cdot \Delta y_v \cdot \Delta z_v)] \quad (B.4)$$

1029 where “S” is the chosen section and “ $N_S$ ” stands for the total number of grid points along the

1030 section. The velocities  $u_s$  and  $v_s$  and corresponding increments ( $dx_u$ ,  $dz_u$ ,  $dy_v$  and  $dz_v$ ) are the  
1031 original Arakawa C grid (no interpolation) following the rules for sign and discretization as  
1032 specified in the “cdftransport” routine of the Drakkar CDFTOOLS package ([http://meom-  
1033 group.github.io/code/](http://meom-<br/>1033 group.github.io/code/)). This grid specific computation was necessary to obtain a precise budget  
1034 of the total transport when applied over all frontiers of a sub-region. As previously shown for the  
1035 volumes, summing those transports on all water masses conserves the total transports, either on a  
1036 water column, or a boundary section.

1037

### 1038 References

1039 ● Product/Dataset:

1040 NOAA National Geophysical Data Center. 2009: ETOPO1 1 Arc-Minute Global Relief Model.

1041 NOAA National Centers for Environmental Information.

1042 <https://www.ngdc.noaa.gov/mgg/global/> Accessed September 2021.

1043

1044 Amitai, Y., Ashkenazy, Y., & Gildor, H. (2021). The Effect of the Source of Deep Water in the  
1045 Eastern Mediterranean on Western Mediterranean Intermediate and Deep Water. *Frontiers in  
1046 Marine Science*, 7. <https://doi.org/10.3389/fmars.2020.615975>

1047 Astraldi, M., & Gasparini, G. P. (1994). The Seasonal Characteristics of the Circulation in the  
1048 Tyrrhenian Sea. In *Seasonal and Interannual Variability of the Western Mediterranean Sea*  
1049 (pp. 115–134). American Geophysical Union (AGU). <https://doi.org/10.1029/CE046p0115>

1050 Aznar, R., Sotillo, M. G., Cailleau, S., Lorente, P., Levier, B., Amo-Baladrón, A., et al. (2016).  
1051 Strengths and weaknesses of the CMEMS forecasted and reanalyzed solutions for the Iberia–  
1052 Biscay–Ireland (IBI) waters. *Journal of Marine Systems*, 159, 1–14.  
1053 <https://doi.org/10.1016/j.jmarsys.2016.02.007>

1054 Balmaseda, M. A., Hernandez, F., Storto, A., Palmer, M. D., Alves, O., Shi, L., et al. (2015). The  
1055 Ocean Reanalyses Intercomparison Project (ORA-IP). *Journal of Operational Oceanography*,  
1056 8(sup1), s80–s97. <https://doi.org/10.1080/1755876X.2015.1022329>

1057 Barral, Q.-B., Zakardjian, B., Dumas, F., Garreau, P., & Beuvier, J. (2020). Analysis of specific  
1058 water masses transports in the Western Mediterranean in the MEDRYS1V2 twenty-one-year  
1059 reanalysis. <https://doi.org/10.5194/egusphere-egu2020-21979>

1060 Barral, Q.-B., Zakardjian, B., Dumas, F., Garreau, P., Testor, P., & Beuvier, J. (2021).  
1061 Characterization of fronts in the Western Mediterranean with a special focus on the North  
1062 Balearic Front. *Progress in Oceanography*, 197, 102636.  
1063 <https://doi.org/10.1016/j.pocean.2021.102636>

1064 Bauch, D., & Cherniavskaia, E. (2018). Water Mass Classification on a Highly Variable Arctic  
1065 Shelf Region: Origin of Laptev Sea Water Masses and Implications for the Nutrient Budget.  
1066 *Journal of Geophysical Research: Oceans*, 123(3), 1896–1906.  
1067 <https://doi.org/10.1002/2017JC013524>

1068 Ben Ismail, S., Schroeder, K., Sammari, C., Gasparini, G. P., Borghini, M., & Aleya, L. (2014).  
1069 Interannual variability of water mass properties in the Tunisia–Sicily Channel. *Journal of  
1070 Marine Systems*, 135, 14–28. <https://doi.org/10.1016/j.jmarsys.2013.06.010>

- 1071 Ben Ismail, S., Schroeder, K., Chiggiato, J., Sparnocchia, S., Borghini, M. (2021). Long term  
1072 changes monitored in two Mediterranean Channels. in von Schuckmann et al., (2021)  
1073 Copernicus Marine Service Ocean State Report, Issue 5, *Journal of Operational*  
1074 *Oceanography*, 14:sup1, 1-185, <https://doi.org/10.1080/1755876X.2021.1946240>
- 1075 Bensoussan, N., Cebrian, E., Dominici, J.-M., Kersting D.-K., Kipson, S., Kizilkaya, Z., Ocaña,  
1076 O., Peirache, M., Zuberer, F., Ledoux, J.-B., Linares, C., Zabala, M., Buongiorno Nardelli, B.,  
1077 Pisano, A., & Garrabou, J. (2019). Using CMEMS and the Mediterranean Marine Protected  
1078 Areas sentinel network to track ocean warming effects in coastal areas. in von Schuckmann et  
1079 al., (2019) Copernicus Marine Service Ocean State Report, Issue 3, *Journal of Operational*  
1080 *Oceanography*, 12:sup1, S1-S123, <https://doi.org/10.1080/1755876X.2019.1633075>
- 1081 Béranger, K., Mortier, L., Gasparini, G.-P., Gervasio, L., Astraldi, M., & Crépon, M. (2004). The  
1082 dynamics of the Sicily Strait: a comprehensive study from observations and models. *Deep Sea*  
1083 *Research Part II: Topical Studies in Oceanography*, 51(4–5), 411–440.  
1084 <https://doi.org/10.1016/j.dsr2.2003.08.004>
- 1085 Béranger, K., Mortier, L., & Crépon, M. (2005). Seasonal variability of water transport through  
1086 the Straits of Gibraltar, Sicily and Corsica, derived from a high-resolution model of the  
1087 Mediterranean circulation. *Progr. Oceanogr.*, 66(2–4), 341–364.  
1088 <https://doi.org/10.1016/j.pocean.2004.07.013>
- 1089 Bergamasco, A., & Malanotte-Rizzoli, P. (2010). The circulation of the Mediterranean Sea: a  
1090 historical review of experimental investigations. *Advances in Oceanography and Limnology*,  
1091 1(1), 11–28. <https://doi.org/10.1080/19475721.2010.491656>
- 1092 Bethoux, J. (1980). Mean water fluxes across sections in the mediterranean-sea, evaluated on the  
1093 basis of water and salt budgets and of observed salinities. *Oceanologica Acta*, 3(1), 79–88.
- 1094 Bethoux, J. P., & Gentili, B. (1999). Functioning of the Mediterranean Sea: past and present  
1095 changes related to freshwater input and climate changes. *Journal of Marine Systems*, 20(1–4),  
1096 33–47. [https://doi.org/10.1016/S0924-7963\(98\)00069-4](https://doi.org/10.1016/S0924-7963(98)00069-4)
- 1097 Bethoux, J. P., Prieur, L., & Nyffeler, F. (1982). The Water Circulation in the North-Western  
1098 Mediterranean Sea, its Relations with Wind and Atmospheric Pressure. In J. C. J. Nihoul  
1099 (Ed.), *Elsevier Oceanography Series* (Vol. 34, pp. 129–142). Elsevier.  
1100 [https://doi.org/10.1016/S0422-9894\(08\)71240-6](https://doi.org/10.1016/S0422-9894(08)71240-6)
- 1101 Bethoux, J. P., Gentili, B., Morin, P., Nicolas, E., Pierre, C., & Ruiz-Pino, D. (1999). The  
1102 Mediterranean Sea: a miniature ocean for climatic and environmental studies and a key for the  
1103 climatic functioning of the North Atlantic. *Progress in Oceanography*, 44(1–3), 131–146.  
1104 [https://doi.org/10.1016/S0079-6611\(99\)00023-3](https://doi.org/10.1016/S0079-6611(99)00023-3)
- 1105 Béthoux, J.-P., Gentili, B., & Tailliez, D. (1998). Warming and freshwater budget change in the  
1106 Mediterranean since the 1940s, their possible relation to the greenhouse effect. *Geophysical*  
1107 *Research Letters*, 25(7), 1023–1026. <https://doi.org/10.1029/98GL00724>
- 1108 Beuvier, J., Béranger, K., Lebeaupin Brossier, C., Somot, S., Sevault, F., Drillet, Y., et al. (2012).  
1109 Spreading of the Western Mediterranean Deep Water after winter 2005: Time scales and deep  
1110 cyclone transport. *Journal of Geophysical Research: Oceans*, 117(C7), n/a-n/a.  
1111 <https://doi.org/10.1029/2011JC007679>
- 1112 Beuvier, J., Hamon, M., Greiner, E., Drévilion, M., & Lellouche, J. (2016). New Version of

- 1113 MEDRYS, A Mediterranean Sea Reanalysis During 1992-2013, Rapp. Comm. Int. Mer Medit.  
1114 Vol.41 p.123, Proceedings of the 41th CIESM Congress, Kiel, Germany, september 2016.
- 1115 Borghini, M., Bryden, H., Schroeder, K., Sparnocchia, S., & Vetrano, A. (2014). The  
1116 Mediterranean is becoming saltier. *Ocean Science*, *10*(4), 693–700. [https://doi.org/10.5194/os-](https://doi.org/10.5194/os-10-693-2014)  
1117 [10-693-2014](https://doi.org/10.5194/os-10-693-2014)
- 1118 Bosse, A., Testor, P., Mortier, L., Prieur, L., Taillandier, V., d’Ortenzio, F., & Coppola, L. (2015).  
1119 Spreading of Levantine Intermediate Waters by submesoscale coherent vortices in the  
1120 northwestern Mediterranean Sea as observed with gliders. *Journal of Geophysical Research:*  
1121 *Oceans*, *120*(3), 1599–1622. <https://doi.org/10.1002/2014JC010263>
- 1122 Bosse, A., Testor, P., Houpert, L., Damien, P., Prieur, L., Hayes, D., et al. (2016). Scales and  
1123 dynamics of Submesoscale Coherent Vortices formed by deep convection in the northwestern  
1124 Mediterranean Sea. *Journal of Geophysical Research: Oceans*, *121*(10), 7716–7742.  
1125 <https://doi.org/10.1002/2016JC012144>
- 1126 de Brauwere, A., Jacquet, S. H. M., De Ridder, F., Dehairs, F., Pintelon, R., Schoukens, J., &  
1127 Baeyens, W. (2007). Water mass distributions in the Southern Ocean derived from a  
1128 parametric analysis of mixing water masses. *Journal of Geophysical Research*, *112*(C2),  
1129 C02021. <https://doi.org/10.1029/2006JC003742>
- 1130 Bryden, H. L., Candela, J., & Kinder, T. H. (1994). Exchange through the Strait of Gibraltar.  
1131 *Progress in Oceanography*, *33*(3), 201–248. [https://doi.org/10.1016/0079-6611\(94\)90028-0](https://doi.org/10.1016/0079-6611(94)90028-0)
- 1132 Buffett, G. G., Krahnmann, G., Klaeschen, D., Schroeder, K., Sallarès, V., Papenberg, C., et al.  
1133 (2017). Seismic Oceanography in the Tyrrhenian Sea: Thermohaline Staircases, Eddies, and  
1134 Internal Waves. *Journal of Geophysical Research: Oceans*, *122*(11), 8503–8523.  
1135 <https://doi.org/10.1002/2017JC012726>
- 1136 Cabanes, C., Grouazel, A., Schuckmann, K. von, Hamon, M., Turpin, V., Coatanoan, C., et al.  
1137 (2013). The CORA dataset: validation and diagnostics of in-situ ocean temperature and  
1138 salinity measurements. *Ocean Science*, *9*(1), 1–18. <https://doi.org/10.5194/os-9-1-2013>
- 1139 Cacho, I., Grimalt, J. O., Sierro, F. J., Shackleton, N., & Canals, M. (2000). Evidence for  
1140 enhanced Mediterranean thermohaline circulation during rapid climatic coolings. *Earth and*  
1141 *Planetary Science Letters*, *183*(3–4), 417–429. [https://doi.org/10.1016/S0012-](https://doi.org/10.1016/S0012-821X(00)00296-X)  
1142 [821X\(00\)00296-X](https://doi.org/10.1016/S0012-821X(00)00296-X)
- 1143 Cacho, I., Grimalt, J. O., Canals, M., Sbaiffi, L., Shackleton, N. J., Schönfeld, J., & Zahn, R.  
1144 (2001). Variability of the western Mediterranean Sea surface temperature during the last  
1145 25,000 years and its connection with the Northern Hemisphere climatic changes.  
1146 *Paleoceanography*, *16*(1), 40–52. <https://doi.org/10.1029/2000PA000502>
- 1147 Cardin, V., & Celio, M. (1997). Cluster analysis as a statistical method for identification of the  
1148 water bodies present in the Gulf of Trieste (Northern Adriatic Sea), 17.
- 1149 Cardin, V., Civitarese, G., Hainbucher, D., Bensi, M., & Rubino, A. (2015). Thermohaline  
1150 properties in the Eastern Mediterranean in the last three decades: is the basin returning to the  
1151 pre-EMT situation? *Ocean Science*, *11*(1), 53–66. <https://doi.org/10.5194/os-11-53-2015>
- 1152 Carracedo, L. I., Gilcoto, M., Mercier, H., & Pérez, F. F. (2014). Seasonal dynamics in the  
1153 Azores–Gibraltar Strait region: A climatologically-based study. *Progress in Oceanography*,

- 1154 122, 116–130. <https://doi.org/10.1016/j.pocean.2013.12.005>
- 1155 CIESM, 2001. Round table session on Mediterranean water mass acronyms. 36th CIESM  
1156 Congress, Monte Carlo, 26 September 2001 [http://ciesm.org/events/RT5-](http://ciesm.org/events/RT5-WaterMassAcronyms.pdf)  
1157 [WaterMassAcronyms.pdf](http://ciesm.org/events/RT5-WaterMassAcronyms.pdf)
- 1158 CIESM, 2002. Tracking long-term hydrological change in the Mediterranean Sea. Workshop  
1159 Series, n°16, <http://www.ciesm.org/online/monographs/Monaco02.html>
- 1160 Colin, J., Déqué, M., Radu, R., & Somot, S. (2010). Sensitivity study of heavy precipitation in  
1161 Limited Area Model climate simulations: influence of the size of the domain and the use of  
1162 the spectral nudging technique. *Tellus A: Dynamic Meteorology and Oceanography*, 62(5),  
1163 591–604. <https://doi.org/10.1111/j.1600-0870.2010.00467.x>
- 1164 Cortina-Guerra, A., Gomez-Navarro, J. J., Martrat, B., Montávez, J. P., Incarbona, A., Grimalt, J.  
1165 O., et al. (2021). Northern Hemisphere atmospheric pattern enhancing Eastern Mediterranean  
1166 Transient-type events during the past 1000 years. *Climate of the Past*, 17(4), 1523–1532.  
1167 <https://doi.org/10.5194/cp-17-1523-2021>
- 1168 Crépon, M., & Boukthir, M. (1987). Effect of deep water formation on the circulation of the  
1169 Ligurian Sea. *Effect of Deep Water Formation on the Circulation of the Ligurian Sea*, 5(1),  
1170 43–48.
- 1171 Dee, D. P., Uppala, S. M., Simmons, A. J., Berrisford, P., Poli, P., Kobayashi, S., et al. (2011).  
1172 The ERA-Interim reanalysis: configuration and performance of the data assimilation system.  
1173 *Quarterly Journal of the Royal Meteorological Society*, 137(656), 553–597.  
1174 <https://doi.org/10.1002/qj.828>
- 1175 Escudier, R., Mourre, B., Juza, M., & Tintoré, J. (2016). Subsurface circulation and mesoscale  
1176 variability in the Algerian subs basin from altimeter-derived eddy trajectories. *Journal of*  
1177 *Geophysical Research: Oceans*, 121(8), 6310–6322. <https://doi.org/10.1002/2016JC011760>
- 1178 Escudier, R., Clementi, E., Cipollone, A., Pistoia, J., Drudi, M., Grandi, A., et al. (2021). A High  
1179 Resolution Reanalysis for the Mediterranean Sea. *Frontiers in Earth Science*, 9, 1060.  
1180 <https://doi.org/10.3389/feart.2021.702285>
- 1181 Falco, P., Trani, M., & Zambianchi, E. (2016). Water mass structure and deep mixing processes  
1182 in the Tyrrhenian Sea: Results from the VECTOR project. *Deep Sea Research Part I:*  
1183 *Oceanographic Research Papers*, 113, 7–21. <https://doi.org/10.1016/j.dsr.2016.04.002>
- 1184 Fedele, G., Mauri, E., Notarstefano, G., & Poulain, P. M. (2022). Characterization of the Atlantic  
1185 Water and Levantine Intermediate Water in the Mediterranean Sea using 20 years of Argo  
1186 data. *Ocean Science*, 18(1), 129–142. <https://doi.org/10.5194/os-18-129-2022>
- 1187 Font, J., Puig, P., Salat, J., Palanques, A., & Emelianov, M. (2007). Sequence of hydrographic  
1188 changes in NW Mediterranean deep water due to the exceptional winter of 2005. *Scientia*  
1189 *Marina*, 71(2), 339–346. <https://doi.org/10.3989/scimar.2007.71n2339>
- 1190 Fox-Kemper, B., Adcroft, A., Böning, C. W., Chassignet, E. P., Curchitser, E., Danabasoglu, G.,  
1191 et al. (2019). Challenges and Prospects in Ocean Circulation Models. *Frontiers in Marine*  
1192 *Science*, 0. <https://doi.org/10.3389/fmars.2019.00065>
- 1193 Fuda, J. L., Millot, C., Taupier-Letage, I., Send, U., & Bocognano, J. M. (2000). XBT monitoring  
1194 of a meridian section across the western Mediterranean Sea. *Deep Sea Research Part I:*

- 1195 *Oceanographic Research Papers*, 47(11), 2191–2218. <https://doi.org/10.1016/S0967->  
1196 0637(00)00018-2
- 1197 Fuda, J.-L., Etiope, G., Millot, C., Favali, P., Calcara, M., Smriglio, G., & Boschi, E. (2002).  
1198 Warming, salting and origin of the Tyrrhenian Deep Water: Warming, salting and origin of the  
1199 tyrrhenian deep water. *Geophysical Research Letters*, 29(19), 4-1-4-4.  
1200 <https://doi.org/10.1029/2001GL014072>
- 1201 Gačić, M., Schroeder, K., Civitarese, G., Cosoli, S., Vetrano, A., & Eusebi Borzelli, G. L. (2013).  
1202 Salinity in the Sicily Channel corroborates the role of the Adriatic–Ionian Bimodal Oscillating  
1203 System (BiOS) in shaping the decadal variability of the Mediterranean overturning  
1204 circulation. *Ocean Science*, 9(1), 83–90. <https://doi.org/10.5194/os-9-83-2013>
- 1205 Gao, Y., Huang, R. X., Zhu, J., Huang, Y., & Hu, J. (2020). Using the Sigma-Pi Diagram to  
1206 Analyze Water Masses in the Northern South China Sea in Spring. *Journal of Geophysical*  
1207 *Research: Oceans*, 125(7), e2019JC015676. <https://doi.org/10.1029/2019JC015676>
- 1208 García-Herrera, R., Díaz, J., Trigo, R. M., Luterbacher, J., & Fischer, E. M. (2010). A Review of  
1209 the European Summer Heat Wave of 2003. *Critical Reviews in Environmental Science and*  
1210 *Technology*, 40(4), 267–306. <https://doi.org/10.1080/10643380802238137>
- 1211 Gasparini, G. P., Ortona, A., Budillon, G., Astraldi, M., & Sansone, E. (2005). The effect of the  
1212 Eastern Mediterranean Transient on the hydrographic characteristics in the Strait of Sicily and  
1213 in the Tyrrhenian Sea. *Deep Sea Research Part I: Oceanographic Research Papers*, 52(6),  
1214 915–935. <https://doi.org/10.1016/j.dsr.2005.01.001>
- 1215 Hamon, M., Beuvier, J., Somot, S., Lellouche, J.-M., Greiner, E., Jordà, G., et al. (2016). Design  
1216 and validation of MEDRYS, a Mediterranean Sea reanalysis over the period 1992–2013.  
1217 *Ocean Science*, 12(2), 577–599. <https://doi.org/10.5194/os-12-577-2016>
- 1218 Hassoun, A. E. R., Guglielmi, V., Gemayel, E., Goyet, C., Saab, M. A.-A., Giani, M., et al.  
1219 (2015). Is the Mediterranean Sea Circulation in a Steady State. *Journal of Water Resources*  
1220 *and Ocean Science*, 4(1), 6. <https://doi.org/10.11648/j.wros.20150401.12>
- 1221 Herrmann, M., Estournel, C., Déqué, M., Marsaleix, P., Sevault, F., & Somot, S. (2008). Dense  
1222 water formation in the Gulf of Lions shelf: Impact of atmospheric interannual variability and  
1223 climate change. *Continental Shelf Research*, 28(15), 2092–2112.  
1224 <https://doi.org/10.1016/j.csr.2008.03.003>
- 1225 Herrmann, M., Sevault, F., Beuvier, J., & Somot, S. (2010). What induced the exceptional 2005  
1226 convection event in the northwestern Mediterranean basin? Answers from a modeling study.  
1227 *Journal of Geophysical Research: Oceans*, 115(C12). <https://doi.org/10.1029/2010JC006162>
- 1228 Hjelmervik, K. T., & Hjelmervik, K. (2013). Estimating temperature and salinity profiles using  
1229 empirical orthogonal functions and clustering on historical measurements. *Ocean Dynamics*,  
1230 63(7), 809–821. <https://doi.org/10.1007/s10236-013-0623-3>
- 1231 Houpert, L., Durrieu de Madron, X., Testor, P., Bosse, A., D’Ortenzio, F., Bouin, M. N., et al.  
1232 (2016). Observations of open-ocean deep convection in the northwestern Mediterranean Sea:  
1233 Seasonal and interannual variability of mixing and deep water masses for the 2007–2013  
1234 Period. *Journal of Geophysical Research: Oceans*, 121(11), 8139–8171.  
1235 <https://doi.org/10.1002/2016JC011857>

- 1236 Iacono, R., Napolitano, E., Palma, M., & Sannino, G. (2021). The Tyrrhenian Sea Circulation: A  
1237 Review of Recent Work. *Sustainability*, *13*(11), 6371. <https://doi.org/10.3390/su13116371>
- 1238 Incarbona, A., Martrat, B., Mortyn, P. G., Sprovieri, M., Ziveri, P., Gogou, A., et al. (2016).  
1239 Mediterranean circulation perturbations over the last five centuries: Relevance to past Eastern  
1240 Mediterranean Transient-type events. *Scientific Reports*, *6*(1), 29623.  
1241 <https://doi.org/10.1038/srep29623>
- 1242 Iona, A., Theodorou, A., Sofianos, S., Watelet, S., Troupin, C., & Beckers, J.-M. (2018).  
1243 Mediterranean Sea climatic indices: monitoring long-term variability and climate changes.  
1244 *Earth System Science Data*, *10*(4), 1829–1842. <https://doi.org/10.5194/essd-10-1829-2018>
- 1245 Isern-Fontanet, J., García-Ladona, E., & Font, J. (2006). Vortices of the Mediterranean Sea: An  
1246 Altimetric Perspective. *Journal of Physical Oceanography*, *36*(1), 87–103.  
1247 <https://doi.org/10.1175/JPO2826.1>
- 1248 Jebri, F., Birol, F., Zakardjian, B., Bouffard, J., & Sammari, C. (2016). Exploiting coastal  
1249 altimetry to improve the surface circulation scheme over the central Mediterranean Sea.  
1250 *Journal of Geophysical Research: Oceans*, *121*(7), 4888–4909.  
1251 <https://doi.org/10.1002/2016JC011961>
- 1252 Juza, M., Renault, L., Ruiz, S., & Tintoré, J. (2013). Origin and pathways of Winter Intermediate  
1253 Water in the Northwestern Mediterranean Sea using observations and numerical simulation:  
1254 Origin and Pathways of Wiw in Nwmed. *Journal of Geophysical Research: Oceans*, *118*(12),  
1255 6621–6633. <https://doi.org/10.1002/2013JC009231>
- 1256 Juza, M., Mourre, B., Lellouche, J.-M., Tonani, M., & Tintoré, J. (2015). From basin to sub-basin  
1257 scale assessment and intercomparison of numerical simulations in the Western Mediterranean  
1258 Sea. *Journal of Marine Systems*, *149*, 36–49. <https://doi.org/10.1016/j.jmarsys.2015.04.010>
- 1259 Juza, M., Escudier, R., Vargas-Yáñez, M., Mourre, B., Heslop, E., Allen, J., & Tintoré, J. (2019).  
1260 Characterization of changes in Western Intermediate Water properties enabled by an  
1261 innovative geometry-based detection approach. *Journal of Marine Systems*, *191*, 1–12.  
1262 <https://doi.org/10.1016/j.jmarsys.2018.11.003>
- 1263 Kim, K., Kim, K.-R., Rhee, T. S., Rho, H. K., Limeburner, R., & Beardsley, R. C. (1991).  
1264 Identification of Water Masses in the Yellow Sea and the East China Sea by Cluster Analysis.  
1265 In K. Takano (Ed.), *Elsevier Oceanography Series* (Vol. 54, pp. 253–267). Elsevier.  
1266 [https://doi.org/10.1016/S0422-9894\(08\)70100-4](https://doi.org/10.1016/S0422-9894(08)70100-4)
- 1267 Knoll, M., Borrione, I., Fiekas, H.-V., Funk, A., Hemming, M. P., Kaiser, J., et al. (2017).  
1268 Hydrography and circulation west of Sardinia in June 2014. *Ocean Science*, *13*(6), 889–904.  
1269 <https://doi.org/10.5194/os-13-889-2017>
- 1270 Krahnmann, G., & Schott, F. (1998). Longterm increases in western Mediterranean salinities and  
1271 temperatures: Anthropogenic and climatic sources. *Geophysical Research Letters*, *25*(22),  
1272 4209–4212. <https://doi.org/10.1029/1998GL900143>
- 1273 Kubin, E., Poulain, P.-M., Mauri, E., Menna, M., & Notarstefano, G. (2019). Levantine  
1274 Intermediate and Levantine Deep Water Formation: An Argo Float Study from 2001 to 2017.  
1275 *Water*, *11*(9), 1781. <https://doi.org/10.3390/w11091781>
- 1276 Lellouche, J.-M., Le Galloudec, O., Drévillon, M., Régnier, C., Greiner, E., Garric, G., et al.



- 1277 (2013). Evaluation of global monitoring and forecasting systems at Mercator Océan. *Ocean*  
1278 *Science*, 9(1), 57–81. <https://doi.org/10.5194/os-9-57-2013>
- 1279 Li, P., & Tanhua, T. (2020). Recent Changes in Deep Ventilation of the Mediterranean Sea;  
1280 Evidence From Long-Term Transient Tracer Observations. *Frontiers in Marine Science*, 7,  
1281 594. <https://doi.org/10.3389/fmars.2020.00594>
- 1282 López-Jurado, J.-L., González-Pola, C., & Vélez-Belchí, P. (2005). Observation of an abrupt  
1283 disruption of the long-term warming trend at the Balearic Sea, western Mediterranean Sea, in  
1284 summer 2005. *Geophysical Research Letters*, 32(24). <https://doi.org/10.1029/2005GL024430>
- 1285 Madec, G., Delecluse, P., Crepon, M., & Chartier, M. (1991). A Three-Dimensional Numerical  
1286 Study of Deep-Water Formation in the Northwestern Mediterranean Sea. *Journal of Physical*  
1287 *Oceanography*, 21(9), 1349–1371. [https://doi.org/10.1175/1520-0485\(1991\)021<1349:ATDNSO>2.0.CO;2](https://doi.org/10.1175/1520-0485(1991)021<1349:ATDNSO>2.0.CO;2)
- 1289 Mallil, K., Testor, P., Bosse, A., Margirier, F., Houpert, L., Le Goff, H., et al. (2021). The  
1290 Levantine Intermediate Water in the western Mediterranean and its interactions with the  
1291 Algerian Gyres: insights from 60 years of observation. *Ocean Science Discussions*, 1–26.  
1292 <https://doi.org/10.5194/os-2021-120>
- 1293 Manca, B. B., Ibello, V., Pacciaroni, M., Scarazzato, P., & Giorgetti, A. (2006). Ventilation of  
1294 deep waters in the Adriatic and Ionian Seas following changes in thermohaline circulation of  
1295 the Eastern Mediterranean. *Climate Research*, 31(2–3), 239–256.  
1296 <https://doi.org/10.3354/cr031239>
- 1297 Manzella, G. M. R., & La Violette, P. E. (1990). The seasonal variation of water mass content in  
1298 the western Mediterranean and its relationship with the inflows through the straits of Gibraltar  
1299 and Sicily. *Journal of Geophysical Research*, 95(C2), 1623.  
1300 <https://doi.org/10.1029/JC095iC02p01623>
- 1301 Mariotti, A., Struglia, M. V., & Zeng, N. (2002). The Hydrological Cycle in the Mediterranean  
1302 Region and Implications for the Water Budget of the Mediterranean Sea. *Journal of Climate*,  
1303 15, 17.
- 1304 Marty, J. C., & Chiavérini, J. (2010). Hydrological changes in the Ligurian Sea (NW  
1305 Mediterranean, DYFAMED site) during 1995–2007 and biogeochemical consequences.  
1306 *Biogeosciences*, 7(7), 2117–2128. <https://doi.org/10.5194/bg-7-2117-2010>
- 1307 Mason, E., & Pascual, A. (2013). Multiscale variability in the Balearic Sea: An altimetric  
1308 perspective: Balearic Sea Variability. *Journal of Geophysical Research: Oceans*, 118(6),  
1309 3007–3025. <https://doi.org/10.1002/jgrc.20234>
- 1310 MEDOC GROUP. (1970). Observation of Formation of Deep Water in the Mediterranean Sea,  
1311 1969. *Nature*, 227(5262), 1037–1040. <https://doi.org/10.1038/2271037a0>
- 1312 Millot, C. (1987). Circulation in the western mediterranean-sea. *Oceanologica Acta*, 10(2), 143–  
1313 149.
- 1314 Millot, C. (1990). The Gulf of Lions' hydrodynamics. *Continental Shelf Research*, 10(9–11),  
1315 885–894. [https://doi.org/10.1016/0278-4343\(90\)90065-T](https://doi.org/10.1016/0278-4343(90)90065-T)
- 1316 Millot, C. (1999). Circulation in the Western Mediterranean Sea. *Journal of Marine Systems*,  
1317 20(1), 423–442. [https://doi.org/10.1016/S0924-7963\(98\)00078-5](https://doi.org/10.1016/S0924-7963(98)00078-5)

- 1318 Millot, C. (2007). Interannual salinification of the Mediterranean inflow. *Geophysical Research*  
1319 *Letters*, 34(21). <https://doi.org/10.1029/2007GL031179>
- 1320 Millot, C. (2009). Another description of the Mediterranean Sea outflow. *Progress in*  
1321 *Oceanography*, 82(2), 101–124. <https://doi.org/10.1016/j.pocean.2009.04.016>
- 1322 Millot, C. (2013). Levantine Intermediate Water characteristics: an astounding general  
1323 misunderstanding! *Scientia Marina*, 77(2), 217–232.  
1324 <https://doi.org/10.3989/scimar.03518.13A>
- 1325 Millot, C., & Taupier-Letage, I. (2005). Circulation in the Mediterranean Sea. In A. Saliot (Ed.),  
1326 *The Mediterranean Sea* (Vol. 5K, pp. 29–66). Berlin, Heidelberg: Springer Berlin Heidelberg.  
1327 <https://doi.org/10.1007/b107143>
- 1328 Millot, C., Candela, J., Fuda, J.-L., & Tber, Y. (2006). Large warming and salinification of the  
1329 Mediterranean outflow due to changes in its composition. *Deep Sea Research Part I:*  
1330 *Oceanographic Research Papers*, 53(4), 656–666. <https://doi.org/10.1016/j.dsr.2005.12.017>
- 1331 Napolitano, E., Iacono, R., Ciuffardi, T., Reseghetti, F., Poulain, P.-M., & Notarstefano, G.  
1332 (2019). The Tyrrhenian Intermediate Water (TIW): Characterization and formation  
1333 mechanisms. *Progress in Oceanography*, 170, 53–68.  
1334 <https://doi.org/10.1016/j.pocean.2018.10.017>
- 1335 Nof, D. (1979). On man-induced variations in the circulation of the Mediterranean Sea. *Tellus*,  
1336 31(6), 558–564. <https://doi.org/10.1111/j.2153-3490.1979.tb00937.x>
- 1337 Nykjaer, L. (2009). Mediterranean Sea surface warming 1985–2006. *Climate Research*, 39, 11–  
1338 17. <https://doi.org/10.3354/cr00794>
- 1339 Olita, A., Sorgente, R., Natale, S., Gaberšek, S., Ribotti, A., Bonanno, A., & Patti, B. (2007).  
1340 Effects of the 2003 European heatwave on the Central Mediterranean Sea: surface fluxes and  
1341 the dynamical response. *Ocean Science*, 3(2), 273–289. <https://doi.org/10.5194/os-3-273-2007>
- 1342 Onken, R., & Sellschopp, J. (2001). Water masses and circulation between the eastern Algerian  
1343 Basin and the Strait of Sicily in October 1996. *Oceanologica Acta*, 24(2), 151–166.  
1344 [https://doi.org/10.1016/S0399-1784\(00\)01135-X](https://doi.org/10.1016/S0399-1784(00)01135-X)
- 1345 Ozer, T., Gertman, I., Kress, N., Silverman, J., & Herut, B. (2017). Interannual thermohaline  
1346 (1979–2014) and nutrient (2002–2014) dynamics in the Levantine surface and intermediate  
1347 water masses, SE Mediterranean Sea. *Global and Planetary Change*, 151, 60–67.  
1348 <https://doi.org/10.1016/j.gloplacha.2016.04.001>
- 1349 Parras-Berrocal, I., Vazquez, R., CabosNarvaez, W. D., Sein, D., Esteban, O. A., Mejías, M. B.,  
1350 & Izquierdo, A. (2021). *Will deep water formation collapse in the North Western*  
1351 *Mediterranean Sea by the end of the 21st century?* (preprint). Earth and Space Science Open  
1352 Archive. Retrieved from <http://www.essoar.org/doi/10.1002/essoar.10507698.1>
- 1353 Peliz, A., Boutov, D., & Teles-Machado, A. (2013). The Alboran Sea mesoscale in a long term  
1354 high resolution simulation: Statistical analysis. *Ocean Modelling*, 72, 32–52.  
1355 <https://doi.org/10.1016/j.ocemod.2013.07.002>
- 1356 Pellet, V., Aires, F., Munier, S., Fernández Prieto, D., Jordá, G., Dorigo, W. A., et al. (2019).  
1357 Integrating multiple satellite observations into a coherent dataset to monitor the full water  
1358 cycle – application to the Mediterranean region. *Hydrology and Earth System Sciences*, 23(1),

- 1359 465–491. <https://doi.org/10.5194/hess-23-465-2019>
- 1360 Pessini, F., Olita, A., Cotroneo, Y., & Perilli, A. (2018). Mesoscale eddies in the Algerian Basin:  
1361 do they differ as a function of their formation site? *Ocean Science*, *14*(4), 669–688.  
1362 <https://doi.org/10.5194/os-14-669-2018>
- 1363 Pinardi, N., Cessi, P., Borile, F., & Wolfe, C. L. P. (2019). The Mediterranean Sea Overturning  
1364 Circulation. *Journal of Physical Oceanography*, *49*(7), 1699–1721.  
1365 <https://doi.org/10.1175/JPO-D-18-0254.1>
- 1366 Piñeiro, S., González-Pola, C., Fernández-Díaz, J. M., & Balbin, R. (2019). Thermohaline  
1367 Evolution of the Western Mediterranean Deep Waters Since 2005: Diffusive Stages and  
1368 Interannual Renewal Injections. *Journal of Geophysical Research: Oceans*, *124*(12), 8747–  
1369 8766. <https://doi.org/10.1029/2019JC015094>
- 1370 Piñeiro, S., González-Pola, C., Fernández-Díaz, J. M., Naveira-Garabato, A. C., Sánchez-Leal,  
1371 R., Puig, P., et al. (2021). Persistent, Depth-Intensified Mixing During The Western  
1372 Mediterranean Transition's Initial Stages. *Journal of Geophysical Research: Oceans*, *126*(2).  
1373 <https://doi.org/10.1029/2020JC016535>
- 1374 Pinot, J.-M., Tintoré, J., & Gomis, D. (1995). Multivariate analysis of the surface circulation in  
1375 the Balearic Sea. *Progress in Oceanography*, *36*(4), 343–376. [https://doi.org/10.1016/0079-](https://doi.org/10.1016/0079-6611(96)00003-1)  
1376 [6611\(96\)00003-1](https://doi.org/10.1016/0079-6611(96)00003-1)
- 1377 Pisano, A., Marullo, S., Artale, V., Falcini, F., Yang, C., Leonelli, F. E., et al. (2020). New  
1378 Evidence of Mediterranean Climate Change and Variability from Sea Surface Temperature  
1379 Observations. *Remote Sensing*, *12*(1), 132. <https://doi.org/10.3390/rs12010132>
- 1380 Prieur, L., Lefevre, D., Gorsky, G., Bianchi, M., Andersen, V., & Gratton, Y. (2003). Frontal  
1381 Processes enhance productivity of the Alboran Sea: a tentative first synthesis of the Almofront  
1382 2 experiment results, 14063. Presented at the EGS - AGU - EUG Joint Assembly.
- 1383 Prieur, Louis, D'ortenzio, F., Taillandier, V., & Testor, P. (2020). Physical Oceanography of the  
1384 Ligurian Sea. In C. Migon, P. Nival, & A. Sciandra (Eds.), *The Mediterranean Sea in the Era*  
1385 *of Global Change 1* (1st ed., pp. 49–78). Wiley. <https://doi.org/10.1002/9781119706960.ch3>
- 1386 Puig, P., Madron, X. D. de, Salat, J., Schroeder, K., Martín, J., Karageorgis, A. P., et al. (2013).  
1387 Thick bottom nepheloid layers in the western Mediterranean generated by deep dense shelf  
1388 water cascading. *Progress in Oceanography*, *111*, 1–23.  
1389 <https://doi.org/10.1016/j.pocean.2012.10.003>
- 1390 Puillat, I., Taupier-Letage, I., & Millot, C. (2002). Algerian Eddies lifetime can near 3 years.  
1391 *Journal of Marine Systems*, *31*(4), 245–259. [https://doi.org/10.1016/S0924-7963\(01\)00056-2](https://doi.org/10.1016/S0924-7963(01)00056-2)
- 1392 Puillat, I., Sorgente, R., Ribotti, A., Natale, S., & Echevin, V. (2006). Westward branching of  
1393 LIW induced by Algerian anticyclonic eddies close to the Sardinian slope. *Chemistry and*  
1394 *Ecology*, *22*(sup1), S293–S305. <https://doi.org/10.1080/02757540600670760>
- 1395 Reynolds, R. W., Smith, T. M., Liu, C., Chelton, D. B., Casey, K. S., & Schlax, M. G. (2007).  
1396 Daily High-Resolution-Blended Analyses for Sea Surface Temperature. *Journal of Climate*,  
1397 *20*(22), 5473–5496. <https://doi.org/10.1175/2007JCLI1824.1>
- 1398 Rhein, M., Send, U., Klein, B., & Krahnemann, G. (1999). Interbasin deep water exchange in the  
1399 western Mediterranean. *Journal of Geophysical Research: Oceans*, *104*(C10), 23495–23508.

- 1400 <https://doi.org/10.1029/1999JC900162>
- 1401 Rio, M. H., Guinehut, S., & Larnicol, G. (2011). New CNES-CLS09 global mean dynamic  
1402 topography computed from the combination of GRACE data, altimetry, and in situ  
1403 measurements. *Journal of Geophysical Research: Oceans*, *116*(C7).  
1404 <https://doi.org/10.1029/2010JC006505>
- 1405 Rixen, M., Beckers, J.-M., Levitus, S., Antonov, J., Boyer, T., Maillard, C., et al. (2005). The  
1406 Western Mediterranean Deep Water: A proxy for climate change. *Geophysical Research  
1407 Letters*, *32*(12). <https://doi.org/10.1029/2005GL022702>
- 1408 Robinson, A. R., & Golnaraghi, M. (1994). The Physical and Dynamical Oceanography of the  
1409 Mediterranean Sea. In P. Malanotte-Rizzoli & A. R. Robinson (Eds.), *Ocean Processes in  
1410 Climate Dynamics: Global and Mediterranean Examples* (pp. 255–306). Dordrecht: Springer  
1411 Netherlands. [https://doi.org/10.1007/978-94-011-0870-6\\_12](https://doi.org/10.1007/978-94-011-0870-6_12)
- 1412 Roether, W., Manca, B. B., Klein, B., Bregant, D., Georgopoulos, D., Beitzel, V., et al. (1996).  
1413 Recent Changes in Eastern Mediterranean Deep Waters. *Science*, *271*(5247), 333–335.  
1414 <https://doi.org/10.1126/science.271.5247.333>
- 1415 Roether, W., Klein, B., Manca, B. B., Theocharis, A., & Kioroglou, S. (2007). Transient Eastern  
1416 Mediterranean deep waters in response to the massive dense-water output of the Aegean Sea  
1417 in the 1990s. *Progress in Oceanography*, *74*(4), 540–571.  
1418 <https://doi.org/10.1016/j.pocean.2007.03.001>
- 1419 Salat, J., & Font, J. (1987). Water mass structure near and offshore the Catalan coast during the  
1420 winters of 1982 and 1983. *Water Mass Structure near and Offshore the Catalan Coast during  
1421 the Winters of 1982 and 1983*, *5*(1), 48–54.
- 1422 Sammari, C., Millot, C., Taupier-Letage, I., Stefani, A., & Brahim, M. (1999). Hydrological  
1423 characteristics in the Tunisia–Sardinia–Sicily area during spring 1995. *Deep Sea Research  
1424 Part I: Oceanographic Research Papers*, *46*(10), 1671–1703. [https://doi.org/10.1016/S0967-  
1425 0637\(99\)00026-6](https://doi.org/10.1016/S0967-0637(99)00026-6)
- 1426 Schauer, U., & Losch, M. (2019). “Freshwater” in the Ocean is Not a Useful Parameter in  
1427 Climate Research. *Journal of Physical Oceanography*, *49*(9), 2309–2321.  
1428 <https://doi.org/10.1175/JPO-D-19-0102.1>
- 1429 Schneider, A., Tanhua, T., Roether, W., & Steinfeldt, R. (2014). Changes in ventilation of the  
1430 Mediterranean Sea during the past 25 year. *Ocean Science*, *10*(1), 1–16.  
1431 <https://doi.org/10.5194/os-10-1-2014>
- 1432 Schröder, K., Gasparini, G. P., Tangherlini, M., & Astraldi, M. (2006). Deep and intermediate  
1433 water in the western Mediterranean under the influence of the Eastern Mediterranean  
1434 Transient. *Geophysical Research Letters*, *33*(21), L21607.  
1435 <https://doi.org/10.1029/2006GL027121>
- 1436 Schroeder, K., Ribotti, A., Borghini, M., Sorgente, R., Perilli, A., & Gasparini, G. P. (2008). An  
1437 extensive western Mediterranean deep water renewal between 2004 and 2006. *Geophysical  
1438 Research Letters*, *35*(18). <https://doi.org/10.1029/2008GL035146>
- 1439 Schroeder, K., Taillandier, V., Vetrano, A., & Gasparini, G. P. (2008). The circulation of the  
1440 western Mediterranean Sea in spring 2005 as inferred from observations and from model

- 1441 outputs. *Deep Sea Research Part I: Oceanographic Research Papers*, 55(8), 947–965.  
1442 <https://doi.org/10.1016/j.dsr.2008.04.003>
- 1443 Schroeder, K., Josey, S. A., Herrmann, M., Grignon, L., Gasparini, G. P., & Bryden, H. L.  
1444 (2010). Abrupt warming and salting of the Western Mediterranean Deep Water after 2005:  
1445 Atmospheric forcings and lateral advection. *Journal of Geophysical Research*, 115(C8),  
1446 C08029. <https://doi.org/10.1029/2009JC005749>
- 1447 Schroeder, K., Chiggiato, J., Bryden, H. L., Borghini, M., & Ben Ismail, S. (2016). Abrupt  
1448 climate shift in the Western Mediterranean Sea. *Scientific Reports*, 6(1), 23009.  
1449 <https://doi.org/10.1038/srep23009>
- 1450 Schroeder, K., Chiggiato, J., Josey, S. A., Borghini, M., Aracri, S., & Sparnocchia, S. (2017).  
1451 Rapid response to climate change in a marginal sea. *Scientific Reports*, 7(1), 4065.  
1452 <https://doi.org/10.1038/s41598-017-04455-5>
- 1453 Schroeder, Katrin, Cozzi, S., Belgacem, M., Borghini, M., Cantoni, C., Durante, S., et al. (2020).  
1454 Along-Path Evolution of Biogeochemical and Carbonate System Properties in the  
1455 Intermediate Water of the Western Mediterranean. *Frontiers in Marine Science*, 7.  
1456 <https://doi.org/10.3389/fmars.2020.00375>
- 1457 Send, U., & Testor, P. (2017). Direct Observations Reveal the Deep Circulation of the Western  
1458 Mediterranean Sea. *Journal of Geophysical Research: Oceans*, 122(12), 10091–10098.  
1459 <https://doi.org/10.1002/2016JC012679>
- 1460 de Sherbinin, A. (2014). Climate change hotspots mapping: what have we learned? *Climatic  
1461 Change*, 123(1), 23–37. <https://doi.org/10.1007/s10584-013-0900-7>
- 1462 Sisma-Ventura, G., Kress, N., Silverman, J., Gertner, Y., Ozer, T., Biton, E., et al. (2021). Post-  
1463 eastern Mediterranean Transient Oxygen Decline in the Deep Waters of the Southeast  
1464 Mediterranean Sea Supports Weakening of Ventilation Rates. *Frontiers in Marine Science*, 7.  
1465 <https://doi.org/10.3389/fmars.2020.598686>
- 1466 Skliris, N., Zika, J. D., Herold, L., Josey, S. A., & Marsh, R. (2018). Mediterranean sea water  
1467 budget long-term trend inferred from salinity observations. *Climate Dynamics*, 51(7–8),  
1468 2857–2876. <https://doi.org/10.1007/s00382-017-4053-7>
- 1469 Somot, S., Sevault, F., & Déqué, M. (2006). Transient climate change scenario simulation of the  
1470 Mediterranean Sea for the twenty-first century using a high-resolution ocean circulation  
1471 model. *Climate Dynamics*, 27(7), 851–879. <https://doi.org/10.1007/s00382-006-0167-z>
- 1472 Somot, S., Sevault, F., Déqué, M., & Crépon, M. (2008). 21st century climate change scenario  
1473 for the Mediterranean using a coupled atmosphere–ocean regional climate model. *Global and  
1474 Planetary Change*, 63(2–3), 112–126. <https://doi.org/10.1016/j.gloplacha.2007.10.003>
- 1475 Somot, Samuel, Jorda, G., Harzallah, A., & Darmaraki, S. (2016). Sub-chapter 1.2.3. The  
1476 Mediterranean Sea in the future climate projections. In J.-P. Moatti & S. Thiébaud (Eds.), *The  
1477 Mediterranean region under climate change* (pp. 93–104). IRD Éditions.  
1478 <https://doi.org/10.4000/books.irdeditions.23100>
- 1479 Somot, Samuel, Houpert, L., Sevault, F., Testor, P., Bosse, A., Taupier-Letage, I., et al. (2018).  
1480 Characterizing, modelling and understanding the climate variability of the deep water  
1481 formation in the North-Western Mediterranean Sea. *Climate Dynamics*, 51(3), 1179–1210.

- 1482 <https://doi.org/10.1007/s00382-016-3295-0>
- 1483 Soto-Navarro, J., Criado-Aldeanueva, F., García-Lafuente, J., & Sánchez-Román, A. (2010).  
1484 Estimation of the Atlantic inflow through the Strait of Gibraltar from climatological and in  
1485 situ data. *Journal of Geophysical Research*, *115*(C10), C10023.  
1486 <https://doi.org/10.1029/2010JC006302>
- 1487 Sparnocchia, S., Gasparini, G. P., Astraldi, M., Borghini, M., & Pistek, P. (1999). Dynamics and  
1488 mixing of the Eastern Mediterranean outflow in the Tyrrhenian basin. *Journal of Marine*  
1489 *Systems*, *20*(1–4), 301–317. [https://doi.org/10.1016/S0924-7963\(98\)00088-8](https://doi.org/10.1016/S0924-7963(98)00088-8)
- 1490 Testor, P., & Gascard, J.-C. (2003). Large-Scale Spreading of Deep Waters in the Western  
1491 Mediterranean Sea by Submesoscale Coherent Eddies. *Journal of Physical Oceanography*,  
1492 *33*(1), 75–87. [https://doi.org/10.1175/1520-0485\(2003\)033<0075:LSSODW>2.0.CO;2](https://doi.org/10.1175/1520-0485(2003)033<0075:LSSODW>2.0.CO;2)
- 1493 Testor, P., Béranger, K., & Mortier, L. (2005). Modeling the deep eddy field in the southwestern  
1494 Mediterranean: The life cycle of Sardinian eddies. *Geophysical Research Letters*, *32*(13).  
1495 <https://doi.org/10.1029/2004GL022283>
- 1496 Testor, P., Send, U., Gascard, J.-C., Millot, C., Taupier-Letage, I., & Béranger, K. (2005). The  
1497 mean circulation of the southwestern Mediterranean Sea: Algerian Gyres. *Journal of*  
1498 *Geophysical Research*, *110*(C11), C11017. <https://doi.org/10.1029/2004JC002861>
- 1499 Testor, Pierre, Bosse, A., Houpert, L., Margirier, F., Mortier, L., Legoff, H., et al. (2018).  
1500 Multiscale Observations of Deep Convection in the Northwestern Mediterranean Sea During  
1501 Winter 2012–2013 Using Multiple Platforms. *Journal of Geophysical Research: Oceans*,  
1502 *123*(3), 1745–1776. <https://doi.org/10.1002/2016JC012671>
- 1503 Theocharis, A., Georgopoulos, D., Lascaratos, A., & Nittis, K. (1993). Water masses and  
1504 circulation in the central region of the Eastern Mediterranean: Eastern Ionian, South Aegean  
1505 and Northwest Levantine, 1986–1987. *Deep Sea Research Part II: Topical Studies in*  
1506 *Oceanography*, *40*(6), 1121–1142. [https://doi.org/10.1016/0967-0645\(93\)90064-T](https://doi.org/10.1016/0967-0645(93)90064-T)
- 1507 Theocharis, Alexander. (2008). Do we expect significant changes in the Thermohaline  
1508 Circulation in the Mediterranean in relation to the observed surface layers warming?, 5.
- 1509 Vara, A. de la, del Sastre, P. G., Arsouze, T., Gallardo, C., & Gaertner, M. Á. (2019). Role of  
1510 atmospheric resolution in the long-term seasonal variability of the Tyrrhenian Sea circulation  
1511 from a set of ocean hindcast simulations (1997–2008). *Ocean Modelling*, *134*, 51–67.  
1512 <https://doi.org/10.1016/j.ocemod.2019.01.004>
- 1513 Vargas-Yáñez, M., Moya, F., García-Martínez, M. C., Tel, E., Zunino, P., Plaza, F., et al. (2010).  
1514 Climate change in the Western Mediterranean Sea 1900–2008. *Journal of Marine Systems*,  
1515 *82*(3), 171–176. <https://doi.org/10.1016/j.jmarsys.2010.04.013>
- 1516 Vargas-Yáñez, M., Zunino, P., Schroeder, K., López-Jurado, J. L., Plaza, F., Serra, M., et al.  
1517 (2012). Extreme Western Intermediate Water formation in winter 2010. *Journal of Marine*  
1518 *Systems*, *105–108*, 52–59. <https://doi.org/10.1016/j.jmarsys.2012.05.010>
- 1519 Vargas-Yáñez, Manuel, Jesús García, M., Salat, J., García-Martínez, M. C., Pascual, J., & Moya,  
1520 F. (2008). Warming trends and decadal variability in the Western Mediterranean shelf. *Global*  
1521 *and Planetary Change*, *63*(2–3), 177–184. <https://doi.org/10.1016/j.gloplacha.2007.09.001>
- 1522 Vargas-Yáñez, Manuel, Juza, M., Balbín, R., Velez-Belchí, P., García-Martínez, M. C., Moya, F.,

- 1523 & Hernández-Guerra, A. (2020). Climatological Hydrographic Properties and Water Mass  
1524 Transports in the Balearic Channels From Repeated Observations Over 1996–2019. *Frontiers*  
1525 *in Marine Science*, 7, 568602. <https://doi.org/10.3389/fmars.2020.568602>
- 1526 Vargas-Yáñez, Manuel, Juza, M., García-Martínez, M. C., Moya, F., Balbín, R., Ballesteros, E.,  
1527 et al. (2021). Long-Term Changes in the Water Mass Properties in the Balearic Channels Over  
1528 the Period 1996–2019. *Frontiers in Marine Science*, 8.  
1529 <https://doi.org/10.3389/fmars.2021.640535>
- 1530 Waldman, R., Somot, S., Herrmann, M., Testor, P., Estournel, C., Sevault, F., et al. (2016).  
1531 Estimating dense water volume and its evolution for the year 2012–2013 in the Northwestern  
1532 Mediterranean Sea: An observing system simulation experiment approach: Estimating dense  
1533 water volume. *Journal of Geophysical Research: Oceans*, 121(9), 6696–6716.  
1534 <https://doi.org/10.1002/2016JC011694>
- 1535 Waldman, R., Herrmann, M., Somot, S., Arsouze, T., Benschila, R., Bosse, A., et al. (2017).  
1536 Impact of the Mesoscale Dynamics on Ocean Deep Convection: The 2012–2013 Case Study  
1537 in the Northwestern Mediterranean Sea. *Journal of Geophysical Research: Oceans*, 122(11),  
1538 8813–8840. <https://doi.org/10.1002/2016JC012587>
- 1539 Waldman, R., Somot, S., Herrmann, M., Bosse, A., Caniaux, G., Estournel, C., et al. (2017).  
1540 Modeling the intense 2012–2013 dense water formation event in the northwestern  
1541 Mediterranean Sea: Evaluation with an ensemble simulation approach: Modeling the 2012–  
1542 2013 DWF event. *Journal of Geophysical Research: Oceans*, 122(2), 1297–1324.  
1543 <https://doi.org/10.1002/2016JC012437>
- 1544 Waldman, R., Somot, S., Herrmann, M., Sevault, F., & Isachsen, P. E. (2018). On the Chaotic  
1545 Variability of Deep Convection in the Mediterranean Sea. *Geophysical Research Letters*,  
1546 45(5), 2433–2443. <https://doi.org/10.1002/2017GL076319>
- 1547 Waldman, R., Brüggemann, N., Bosse, A., Spall, M., Somot, S., & Sevault, F. (2018).  
1548 Overturning the Mediterranean Thermohaline Circulation. *Geophysical Research Letters*,  
1549 45(16), 8407–8415. <https://doi.org/10.1029/2018GL078502>
- 1550 Wüst, G. (1961). On the vertical circulation of the Mediterranean Sea. *Journal of Geophysical*  
1551 *Research (1896-1977)*, 66(10), 3261–3271. <https://doi.org/10.1029/JZ066i010p03261>
- 1552 Younes, W. A. N., Bensoussan, N., Romano, J.-C., Arlhac, D., & Lafont, M.-G. (2003). Seasonal  
1553 and interannual variations (1996–2000) of the coastal waters east of the Rhone river mouth as  
1554 indicated by the SORCOM series. *Oceanologica Acta*, 26(4), 311–321.  
1555 [https://doi.org/10.1016/S0399-1784\(03\)00037-9](https://doi.org/10.1016/S0399-1784(03)00037-9)
- 1556 Zhu, J., Zheng, Q., Hu, J., Lin, H., Chen, D., Chen, Z., et al. (2019). Classification and 3-D  
1557 distribution of upper layer water masses in the northern South China Sea. *Acta Oceanologica*  
1558 *Sinica*, 38(4), 126–135. <https://doi.org/10.1007/s13131-019-1418-2>
- 1559 Zunino, P., Schroeder, K., Vargas-Yáñez, M., Gasparini, G. P., Coppola, L., García-Martínez, M.  
1560 C., & Moya-Ruiz, F. (2012). Effects of the Western Mediterranean Transition on the resident  
1561 water masses: Pure warming, pure freshening and pure heaving. *Journal of Marine Systems*,  
1562 96–97, 15–23. <https://doi.org/10.1016/j.jmarsys.2012.01.011>